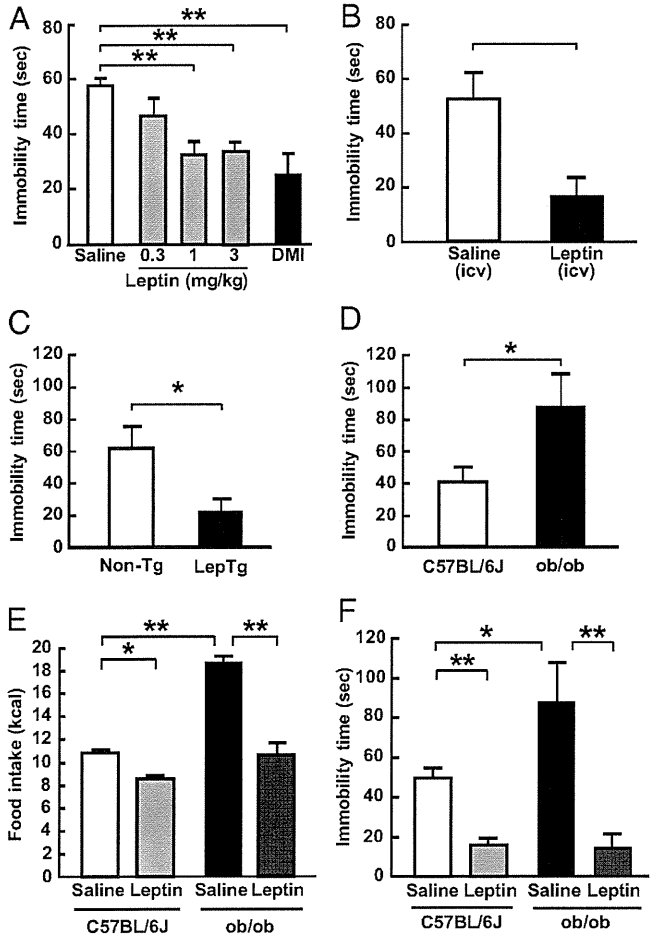

FIG. 1. Effects of leptin on depressive behavior in FST of CD mice, LepTg mice, and ob/ob mice. A, Effect of sc administration of leptin and DMI (7.5 mg/kg) in CD mice on immobility time in the FST. Results are expressed as mean ± SEM for seven to 10 mice. B, Effect of icv administration of leptin (1 μg/2 μl per mouse) on immobility time in CD mice in the FST. Results are expressed as mean ± SEM for eight to 10 mice. C, Depressive behavior in LepTg mice. Results are expressed as mean ± SEM for eight to 10 mice. D, Depressive behavior in C57BL/6J and ob/ob mice. Results are expressed as mean ± SEM for five to eight mice. E, Effect of sc administration of leptin (3 mg/kg) in C57BL/6J and ob/ob mice on nocturnal food intake. Results are expressed as mean ± SEM for 10 mice. F, Antidepressive effect of sc administration of leptin (3 mg/kg) in C57BL/6J and ob/ob mice on immobility time in the FST. Results are expressed as mean ± SEM for five to 10 mice. *, $P < 0.05$; **, $P < 0.01$.

leptin (1 μg/2 μl per mouse), a much smaller dose than the dose of leptin given by sc injection, significantly decreased immobility time of CD mice in the FST without inducing a change in the body weight [saline treatment: pretreatment, 27.4 ± 0.9 g; posttreatment, 26.9 ± 0.6 g; leptin treatment: pretreatment, 30.0 ± 2.3 g; posttreatment, 28.1 ± 1.4 g; $F(3,24) = 1.058$, $P = 0.39$[(Fig. 1B).

To examine whether endogenous leptin is involved in regulating the depressive state, the depressive state in LepTg mice and leptin-deficient ob/ob mice was investigated using the FST. Body weight of LepTg mice (19 ± 0.7 g) was significantly lower than that of control mice [non-Tg; 24 ± 0.6 g; $F(1,16) = 33.47$, $P < 0.01$]. Plasma

TABLE 1. Metabolic parameters of CD and DIO mice

	CD	DIO
Body weight (g)	28.8 ± 0.4	44.7 ± 0.9[a]
Epididymal fat (g)	0.29 ± 0.01	1.58 ± 0.08[a]
Mesenteric fat (g)	0.11 ± 0.01	0.95 ± 0.08[a]
Glucose (ng/dl)	149 ± 8	266 ± 15[a]
Insulin (μU/ml)	21.8 ± 2.9	193.7 ± 29.1[a]
Leptin (ng/ml)	2.3 ± 0.3	41.6 ± 3.0[a]
Triglyceride (mg/dl)	72.6 ± 7.0	79.0 ± 4.2
Corticosterone (μg/dl)	7.22 ± 0.49	7.40 ± 0.73

Results are expressed as mean ± SEM for 16–34 mice.
[a] $P < 0.01$ compared with CD mice.

leptin levels were significantly higher in LepTg mice (65.2 ± 26.0 ng/ml) than in non-Tg mice [7.2 ± 1.9 ng/ml; $F(1,18) = 4.96$, $P < 0.05$]. Plasma leptin levels in LepTg mice were comparable with those in obese humans (27) and DIO mice fed a 60% HFD in the present study (Table 1). The immobility time of LepTg mice in the FST was significantly shorter than that of non-Tg mice (Fig. 1C). In contrast to the LepTg mice, ob/ob mice showed a significant increase in immobility time compared with the control mice (Fig. 1D). The sc administration of leptin (3 mg/kg), which significantly suppressed food intake in both control and ob/ob mice (Fig. 1E), significantly decreased the prolonged immobility time in ob/ob mice without inducing a change in the body weight [saline treatment: pretreatment, 53.4 ± 1.0 g; posttreatment, 53.2 ± 1.0 g; leptin treatment: pretreatment, 53.8 ± 1.2 g; posttreatment, 53.1 ± 1.2 g; $F(3,28) = 0.083$, $P = 0.97$] to a level similar to that caused by leptin treatment in control mice [saline treatment: pretreatment, 25.9 ± 0.5 g; posttreatment, 25.9 ± 0.5 g; leptin treatment: pretreatment, 25.4 ± 0.3 g; posttreatment, 25.1 ± 0.2 g; $F(3,28) = 1.096$, $P = 0.37$] (Fig. 1F).

Depressive behaviors in DIO mice

DIO mice fed a 60% HFD for 16 wk exhibited morbid obesity, hyperglycemia, hyperinsulinemia, and hyperleptinemia (Table 1). The depressive behaviors of DIO mice were examined using both the FST and sucrose preference test in comparison with CD mice. Immobility time of DIO mice without a pretest swimming was very similar to that of CD mice (Fig. 2A). Immobility time of DIO mice without a pretest swimming was very similar to that of CD mice (Fig. 2A), indicating that obesity itself did not influence the immobility time. Moreover, the locomotor activity of DIO mice placed into a new cage for 10 min was the same as that of CD mice (Supplemental Fig. 1). DIO mice exhibited a longer immobility time in the FST compared with CD mice (Fig. 2B). Because of the involvement of hyperactivity of the hypothalamo-pituitary-adrenal axis in depressive behavior (28), plasma corticosterone levels were also com-

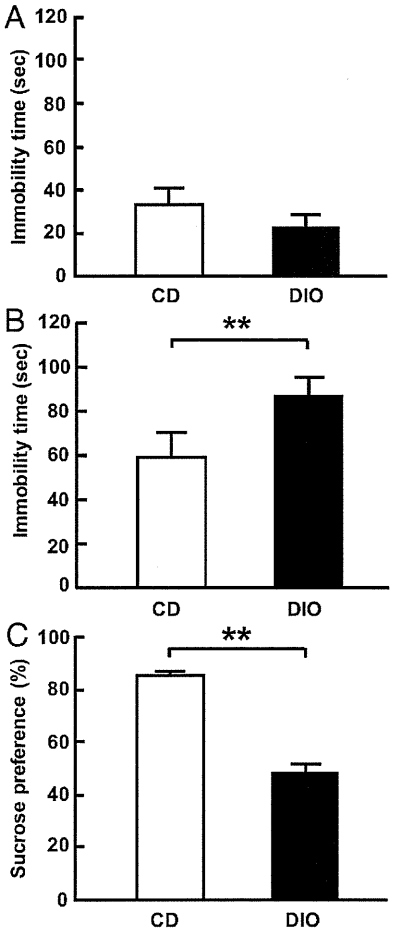

FIG. 2. Depressive behaviors in DIO mice. A, Immobility time in the FST without pretest swimming. Results are expressed as mean ± SEM for six to seven mice. B, Immobility time in the FST. Results are expressed as mean ± SEM for 12–15 mice. C, Preference for sucrose solution. Results are expressed as mean ± SEM for 15 to 16 mice. **, $P < 0.01$.

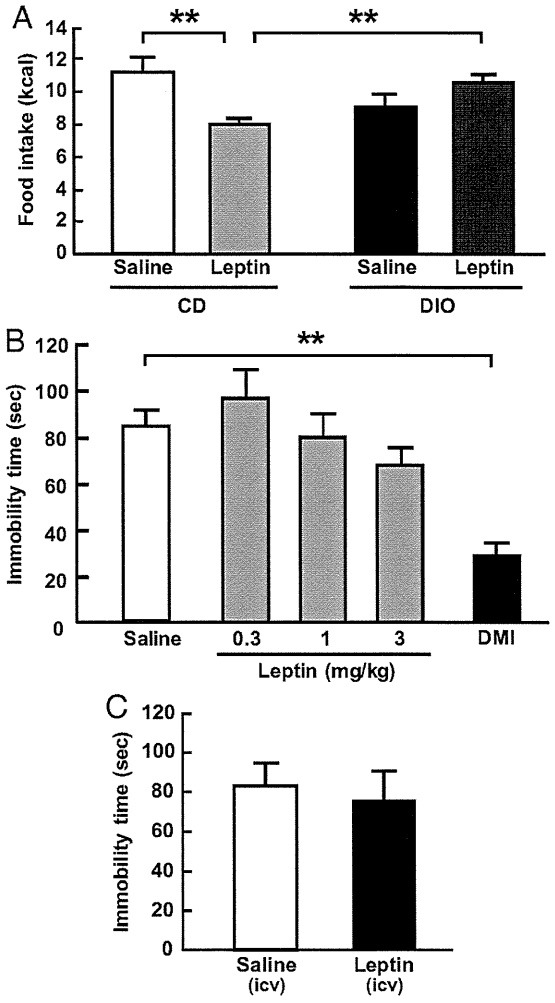

FIG. 3. Effects of leptin in DIO mice on nocturnal food intake and depressive behavior in the FST. A, Effects of sc administration of leptin (3 mg/kg) in CD and DIO mice on nocturnal food intake. Results are expressed as mean ± SEM for five to eight mice. B, Antidepressant effects of sc administration of leptin and DMI (7.5 mg/kg) in DIO mice. Results are expressed as mean ± SEM for five to 16 mice. C, Antidepressive behavior of icv administration of leptin (1 μg/2 μl per mouse) in DIO mice. Results are expressed as mean ± SEM for five to six mice. **, $P < 0.01$.

pared between CD mice and DIO mice. The basal levels of plasma corticosterone in DIO mice were not different from those in CD mice (Table 1). The time course of changes in the plasma corticosterone levels after the pretest swimming in DIO mice was very similar to that observed in CD mice with a peak immediately after the pretest swimming (Supplemental Fig. 2).

The sucrose preference test was performed in CD and DIO mice. DIO mice had a significantly lower preference for the sucrose solution compared with CD mice (Fig. 2C).

Effects of leptin on depressive behavior in DIO mice

The sc administration of leptin (3 mg/kg) significantly suppressed nocturnal food intake in CD mice but not in DIO mice (Fig. 3A). The sc administration of leptin at doses of 1 and 3 mg/kg did not decrease the prolonged immobility time in DIO mice (Fig. 3B), whereas the same doses of leptin significantly decreased immobility time in CD mice (Fig. 1A). In these experiments, leptin treatment did not change body weight in CD mice and DIO mice [DIO mice, saline treatment: pretreatment, 47.8 ± 1.8 g; posttreatment, 47.5 ± 1.7 g; leptin (3 mg/kg) treatment: pretreatment, 48.4 ± 1.0 g; posttreatment, 48.2 ± 1.0 g; $F(3,42) = 0.082$, $P = 0.97$]. In contrast, DMI (7.5 mg/kg) significantly decreased the immobility time in DIO mice (Fig. 3B) without inducing a change in the body weight [DIO mice, saline treatment: pretreatment, 53.1 ± 1.9 g; posttreatment, 52.6 ± 1.9 g; DMI treatment: pretreatment, 51.5 ± 2.0 g; posttreatment, 50.5 ± 2.0 g; $F(3,22) = 0.261$, $P = 0.85$], to a similar extent as that induced by DMI treatment in CD mice (Fig. 1A). Moreover, icv injection of leptin (1 μg/2 μl per mouse) did not decrease the immobility time of DIO mice in the FST (Fig. 3C), whereas the same dose of leptin administered icv induced a significant decease in immobility time in CD mice (Fig. 1B).

TABLE 2. Metabolic parameters in DIO mice after substitution of HFD with CD

	CD/CD	HFD/HFD	HFD/CD
Body weight (g)	31.1 ± 0.4	42.3 ± 1.4[b]	33.9 ± 0.5[a,d]
Epididymal fat (g)	0.31 ± 0.02	1.50 ± 0.15[b]	0.46 ± 0.06[d]
Mesenteric fat (g)	0.23 ± 0.03	0.93 ± 0.13[b]	0.25 ± 0.02[d]
Glucose (ng/dl)	146 ± 11	263 ± 28[b]	148 ± 9[c]
Insulin (μU/ml)	15.2 ± 4.0	171.4 ± 41.5[b]	20.8 ± 8.3[c]
Leptin (ng/ml)	2.9 ± 0.6	51.9 ± 5.3[b]	1.8 ± 1.3[d]
Triglyceride (mg/dl)	88.1 ± 6.7	112.4 ± 10.4	80.7 ± 8.2

CD/CD and HFD/HFD indicate mice kept on CD and HFD, respectively, for 19 wk. HFD/CD indicates mice substituted HFD for 16 wk to CD for another 3 wk. Results are expressed as mean ± SEM for three to 28 mice.

[a] $P < 0.05$ compared with CD/CD mice.

[b] $P < 0.01$ compared with CD/CD mice.

[c] $P < 0.05$ compared with HFD/HFD mice.

[d] $P < 0.01$ compared with HFD/HFD mice.

Effects of substitution of the HFD with the CD on depressive behavior in the FST and leptin activity

To examine whether the increased immobility time of DIO mice in the FST is restored by diet substitution from the HFD to the CD, the diet of the DIO mice was changed from the HFD to the CD for another 3 wk. Diet substitution led to significant reductions in body weight and fat weight and to the normalization of plasma levels of glucose, insulin, and leptin (Table 2). The immobility time in the FST in mice substituted from the HFD to the CD was significantly decreased and identical to that of CD mice (Fig. 4A). Moreover, sc administration of leptin (3 mg/kg) significantly decreased the immobility time of FST in mice substituted from the HFD to the CD (Fig. 4B).

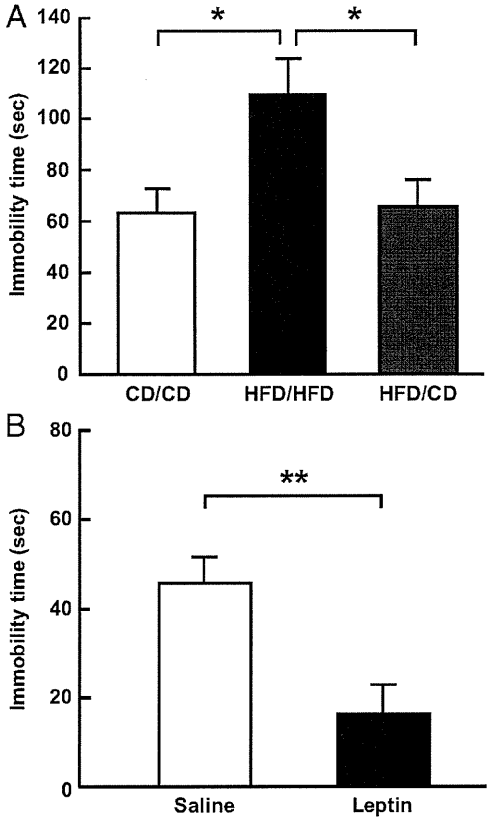

FIG. 4. Effect of substitution of HFD with CD on depressive behavior and leptin activity in the FST. A, Changes in immobility time in DIO mice in the FST after substitution of HFD with CD. CD/CD and HFD/HFD indicate mice kept on CD and HFD, respectively, for 19 wk. HFD/CD indicates mice substituted HFD for 16 wk with CD for another 3 wk. Results are expressed as mean ± SEM for 13–20 mice. B, Effect of sc administration of leptin (3 mg/kg) in mice substituted from the HFD to CD on immobility time in the FST. Results are expressed as mean ± SEM for six mice. *, $P < 0.05$; **, $P < 0.01$.

Changes in the numbers of c-Fos-immunoreactive cells in the hippocampus after sc administration of leptin in CD and DIO mice

The expression of c-Fos, a neuronal activation marker, in the hippocampal CA1–CA3 and DG as well as in the ARC of the hypothalamus was examined after sc administration of leptin (3 mg/kg). The administration of leptin in CD mice markedly increased the number of c-Fos-immunoreactive cells in both the ARC and hippocampal CA3 in comparison with saline treatment (Fig. 5A). In CD mice, leptin significantly increased the number of c-Fos-immunoreactive cells in the ARC and the hippocampal CA1–CA3 and DG by 3.2- and 1.6-fold, respectively, over those after saline treatment in each brain area (Fig. 5, B and C). In contrast to CD mice, leptin did not increase the number of c-Fos-immunoreactive cells in the ARC and hippocampal CA1–CA3 and DG of DIO mice (Fig. 5, B and C). The expression of Ob-Rb mRNA in the hypothalamus and hippocampus in DIO mice was not different from that in CD mice (Fig. 5D).

Involvement of hippocampal BDNF in antidepressive behavior induced by leptin

BDNF concentrations in the hippocampus of DIO mice were significantly decreased by 25% in comparison with CD mice (Fig. 6A). Western blot analysis revealed that full-length TrkB (145 kDa) and truncated form of TrkB (95 kDa) of identical molecular size were detected in the hippocampus of CD mice and DIO mice, respectively (Fig. 6B). There were no changes in the expression of TrkB-fl and TrkB-t in the hippocampus of DIO mice compared with CD mice (Fig. 6B).

BDNF concentrations in the hippocampus of CD and DIO mice were examined after sc administration of leptin (3 mg/kg). Leptin significantly increased the BDNF concentrations by approximately 1.4 times more than those in the hippocampus of CD mice (Fig. 6C). In DIO mice, however, leptin did not affect BDNF concentrations in the hippocampus (Fig. 6C). When BDNF (1 μg/2 μl per mouse) was icv injected in CD and DIO mice, BDNF significantly deceased the immobility time in the FST to a similar extent in both CD and DIO mice (Fig. 6D). In these

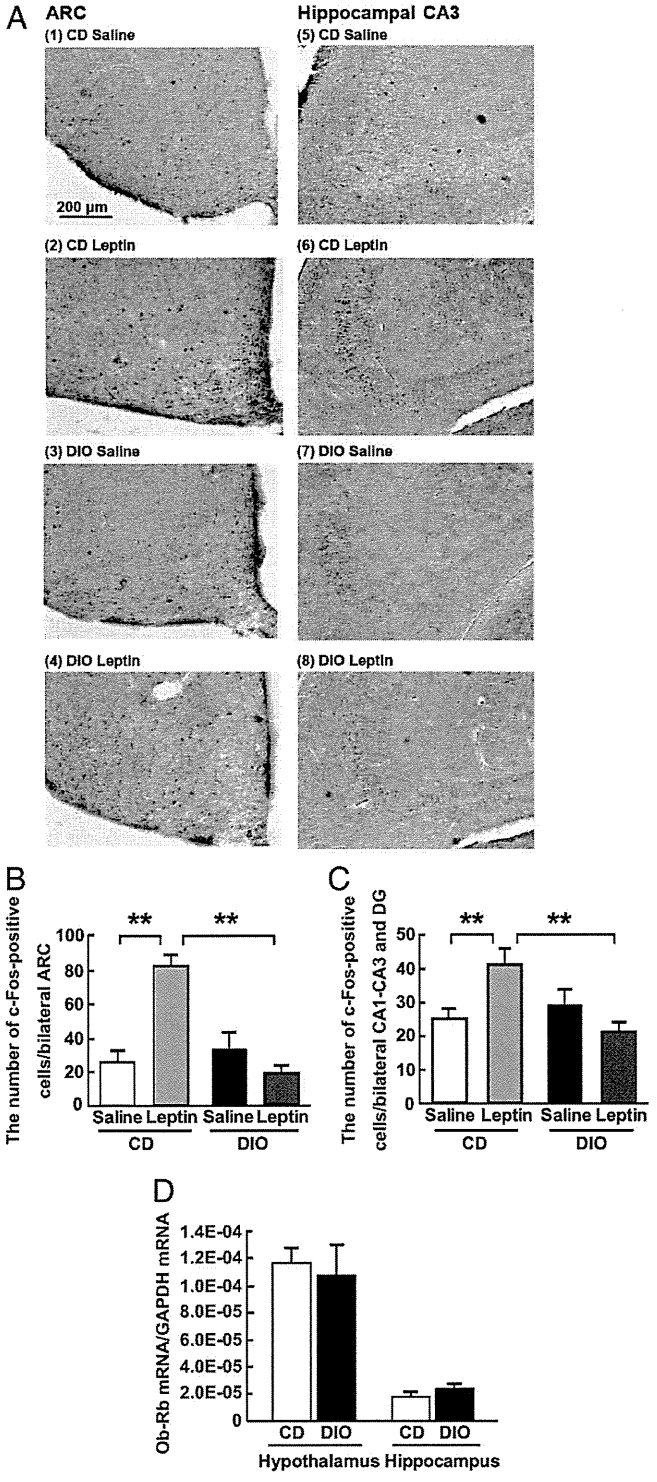

FIG. 5. Changes in the number of c-Fos-immunoreactive cells in the ARC and hippocampus in CD and DIO mice after sc administration of leptin (3 mg/kg). A, Microphotographs of c-Fos-immunoreactive cells in the sections of the ARC [(1) CD Saline, (2) CD Leptin, (3) DIO Saline, and (4) DIO Leptin] and hippocampal CA3 [(5) CD Saline, (6) CD Leptin, (7) DIO Saline, and (8) DIO Leptin] in CD mice and DIO mice. B, The number of c-Fos-immunoreactive cells in the ARC. Results are expressed as mean ± SEM for three to five mice. C, The number of c-Fos-immunoreactive cells in the hippocampal CA1–CA3 and DG. Results are expressed as mean ± SEM for three to five mice. D, Expression of Ob-Rb mRNA in the hypothalamus and hippocampus of CD and DIO mice. Data were presented relative to glyceraldehyde-3-phosphate dehydrogenase (GAPDH) mRNA expression. Results are expressed as mean ± SEM for eight to 10 mice. *, $P < 0.05$; **, $P < 0.01$.

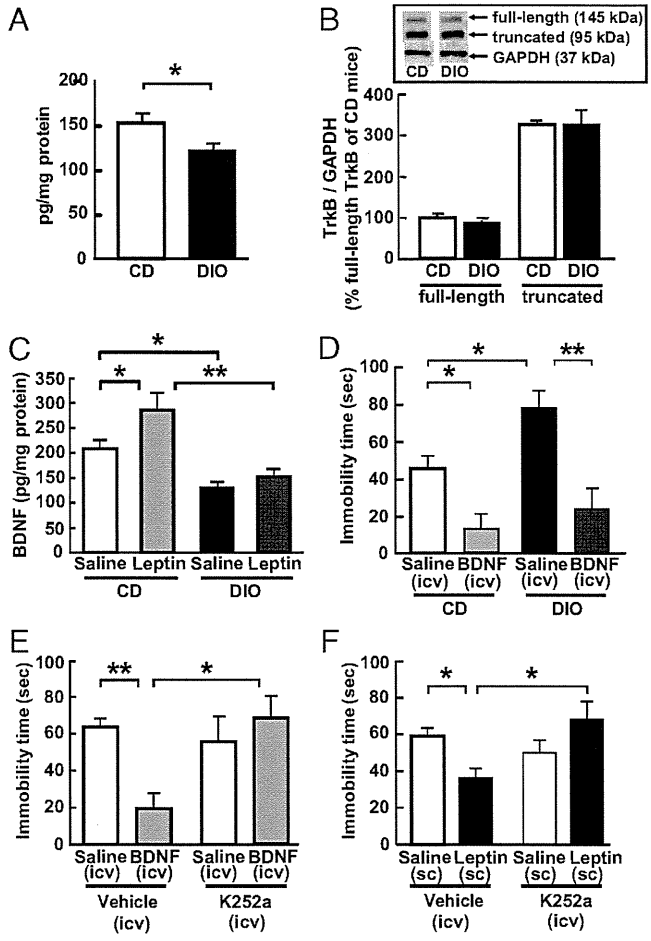

FIG. 6. Involvement of hippocampal BDNF in antidepressive behavior induced by leptin. A, BDNF concentrations in the hippocampus of CD and DIO mice. Results are expressed as mean ± SEM for 17–20 mice. B, Expression of full-length and truncated TrkB receptors in the hippocampus of CD and DIO mice. Western blotting patterns are shown in the *inset*. The figure shows a representation of the densitometry data relative to glyceraldehyde-3-phosphate dehydrogenase (GAPDH) detected in each sample. Results are expressed as mean ± SEM for three mice. C, Effect of sc administration of leptin (3 mg/kg) in CD and DIO mice on the hippocampal BDNF concentrations. Results are expressed as mean ± SEM for 15–18 mice. D, Effect of icv administration of BDNF (1 μg/2 μl per mouse) in CD and DIO mice depressive behavior in the FST. Results are expressed as mean ± SEM for five to eight mice. E, Effect of icv administration of K252a (1 μg/2 μl per mouse) on the antidepressant action induced by icv administration of BDNF (1 μg/2 μl per mouse) in CD mice. Results are expressed as mean ± SEM for six to 11 mice. F, Effect of icv administration of K252a (1 μg/2 μl per mouse) on the antidepressant activity induced by sc injection of leptin (3 mg/kg) in CD mice. Results are expressed as mean ± SEM for five to 10 mice. *, $P < 0.05$; **, $P < 0.01$.

experiments, BDNF treatment did not change body weight in CD mice [saline treatment: pretreatment, 29.2 ± 1.5 g; posttreatment, 28.0 ± 1.3 g; BDNF treatment: pretreatment, 28.0 ± 1.3 g; posttreatment, 26.5 ± 1.3 g; $F(3,32) = 0.460$, $P = 0.71$] and DIO mice [saline treatment: pretreatment, 52.5 ± 1.4 g; posttreatment, 49.7 ± 1.5 g; BDNF treatment: pretreatment, 51.7 ± 1.0 g; posttreatment, 48.9 ± 1.1 g; $F(3,20) = 1.704$, $P = 0.20$].

To examine the involvement of TrkB, BDNF receptor in leptin-induced antidepressive action, we chose K252a for blocking BDNF receptor, TrkB according to a previous report demonstrating that K252a inhibits antidepressant action induced by BDNF (29). The decrease in the immobility time induced by icv injection of BNDF was abolished by icv pretreatment of K252a (1 μg/2 μl per mouse) in CD mice (Fig. 6E). In CD mice icv administered vehicle, immobility time after sc administration of leptin (3 mg/kg) was significantly shorter than that after saline treatment (Fig. 6F). After the concomitant administration of K252a and leptin, the immobility time was significantly longer than that induced by leptin treatment in the vehicle-treated mice, and pretreatment with K252a abolished the antidepressant-like behavior induced by leptin (Fig. 6F).

Discussion

The present study demonstrated that leptin secreted from the adipose tissues has clear antidepressive effects and that DIO mice show more depressive behaviors compared with CD mice. In addition, the present study also demonstrated that DIO mice do not exhibit antidepressive behaviors in response to leptin or show an increased number of c-Fos-immunoreactive cells in the hippocampus as observed in CD mice. These results suggest that the development of depression associated with DIO is, at least in part, due to impaired leptin activity in the hippocampus.

Leptin, an adipokine secreted from the adipocytes, decreases food intake and increases energy expenditure via its actions in the hypothalamus (6). Leptin receptors are highly expressed not only in the hypothalamus but also in various extrahypothalamic brain regions, including the cortex, hippocampus, and amygdala (30, 31), and leptin has widespread biological actions in the central nervous system, such as acting to modulate neuronal development, activity-dependent synaptic plasticity, and learning/memory performance (7, 32–35). The findings of the present study showed that peripheral and central injections of leptin in mice clearly induced significant antidepressive behavior in the FST. Our results are consistent with those of a previous report demonstrating that leptin administration in rats evokes antidepressant-like activity in the FST by its actions in the hippocampus (8). Moreover, in the present study, LepTg mice with high levels of plasma leptin, comparable with those in obese humans and DIO mice, exhibited less depressive behavior in the FST than non-Tg mice, indicating that high plasma leptin levels induce an antidepressive state. In contrast, leptin-deficient ob/ob mice exhibited more depressive behavior in the FST, consistent with a previous report (36). Moreover, in the present study, the severe depressive behavior of ob/ob mice was ameliorated by leptin treatment without changes in body weight. As for the antidepressive action of leptin, the findings obtained in ob/ob mice are mirror image patterns to results observed in LepTg mice.

On the other hand, in the present study, notably, although DIO mice possess increased plasma leptin levels that are comparable with those in LepTg mice, DIO mice exhibited more depressive behavior in the FST than CD mice with no changes in nonspecific motor activity or activation of the hypothalamo-pituitary-adrenal axis, which is considered to induce a depressive state. In addition, a sucrose preference test also demonstrated that DIO mice show depressive behavior. Because it is considered that the FST is stress-induced behavioral despair test (14) and the sucrose preference test reflects the responsiveness to a natural reward (15), these findings obtained in two different experiments evaluating depressive status indicate that DIO mice possess high susceptibility to stress-induced conditions and a depressive state under basal conditions. Central and peripheral administration of leptin did not have antidepressive effects in DIO mice in the FST. Moreover, in response to leptin, DIO mice did not exhibit an increase in the number of c-Fos-immunoreactive cells in the hippocampus, which is considered to be an important brain region for regulation of the depressive state (8), whereas leptin administration in CD mice significantly increased the number of c-Fos immunoreactive cells in the hippocampus. In the present study, however, we did not examine whether leptin directly or indirectly acts on the hippocampus to increase the number of c-Fos-immunoreactive cells in the hippocampus. Leptin resistance results in diminished anorexigenic actions and hypothalamic c-Fos expression in experimental animals with obesity and hyperleptinemia induced by HFD feeding in response to leptin (6, 37), which is consistent with the findings in the present study that leptin did not suppress nocturnal food intake or increase c-Fos expression in the ARC in DIO mice, as it did in CD mice. Taken together, these findings clearly indicate that the DIO mice used in the present study are resistant to the anorexigenic effects of leptin. The findings of the present study suggest that the effects of leptin are impaired in the hippocampus of DIO mice, so-called leptin resistance, resulting in a severe depressive state despite hyperleptinemia.

In the present study, diet substitution from HFD to CD in DIO mice significantly ameliorated the depressive state to a level similar to that in CD mice and restored the antidepressive effects of leptin. This observation is consistent with those of a recent report that diet substitution from HFD to CD in DIO mice restores leptin sensitivity in anorexigenic action (38).

These findings suggest that the development of depression associated with DIO is, in part, due to impaired responses in the hippocampus after leptin treatment. The impaired leptin action in the hippocampus may be involved in cognitive impairment of obesity, because leptin is demonstrated to influence hippocampal-dependent learning and memory (7, 34, 39). In this regard, we reported that DIO mice exhibit cognitive dysfunction in fear conditioning test, including hippocampus and amygdala-dependent responses (40). On the other hand, it is possible that the precise sites of leptin-induced antidepressant action may include other brain regions as well as the hippocampus because of wide distribution of leptin receptors in the central nervous system (30, 31).

BDNF in the hippocampus is considered to play an important role in the control of the depressive state. Injection of BDNF into the hippocampus in experimental animals has antidepressant effects in the FST, and this antidepressant effect induced by BDNF is inhibited by K252a, an inhibitor of the BDNF receptor TrkB (29). BDNF conditional knockout in the mouse forebrain also induces depression-related behavior (17). Moreover, low BDNF levels are reported in the hippocampus of humans with depression (41). The evidence supports the hypothesis that decreased BDNF/TrkB signaling may induce depression (42). In the present study, the hippocampal BDNF concentrations in DIO mice were significantly decreased compared with those of CD mice, whereas the expression of its receptor, TrkB, in the hippocampus was not different between DIO and CD mice. These findings suggest that depression in DIO mice is due to decreased BDNF concentrations in the hippocampus. Furthermore, in the present study, sc administration of leptin significantly increased BDNF concentrations in the hippocampus of CD mice but not in DIO mice. In addition, the antidepressant activity induced by leptin was completely inhibited by the icv administration of K252a in CD mice. These findings indicate that leptin activates the BDNF system in the hippocampus, which in turn, evokes antidepressant activity in CD mice, but DIO mice do not respond to leptin by an increase in the BDNF concentration due to impaired leptin activity in the hippocampus, resulting in a depressive state. However, because K252a is a broad spectrum kinase inhibitor, it is also possible that other kinases, including Janus family of the tyrosine kinase-signal transducers and activators of transcription (JAK-STAT) of downstream of leptin receptor, may be involved in leptin-induced antidepressive action. In the present study, icv administration of BDNF induced potent antidepressant activity in DIO mice to the same extent as that in CD mice. These findings suggest that an impaired BDNF response to leptin in the hippocampus could be involved in the severe depressive behavior observed in DIO mice, although it is not clear whether leptin, directly or indirectly, influences BDNF response in the hippocampus.

Given the high comorbidity of metabolic disorders, such as diabetes and obesity, with depression, several lines of evidence suggest that insulin signaling in the brain is also an important regulator. The clinical investigations show the relationship between insulin resistance and depression (43, 44). Recent study demonstrated that insulin, through the activation of Akt, significantly decreases surface expression of the high-affinity norepinephrine transporter in mouse hippocampal slices, indicating that insulin activates noradrenergic tone in the brain of which decrease is closely related with the development of depression (45). From these findings, insulin resistance is also a candidate for depression associated with obesity. Therefore, further investigation must be needed to elucidate how the interaction between leptin and insulin play an essential role in the development of depression associated with metabolic disorders, such as diabetes and obesity.

The present study demonstrated for the first time that HFDIO mice exhibit a severe depressive state that is, in part, due to impaired leptin activity in the hippocampus and that the antidepressive effects of leptin are mediated by the BDNF/TrkB system in the hippocampus. Further analysis of implication of leptin for depression associated with obesity would provide new insight into the bidirectional interaction between energy regulation and emotion.

Acknowledgments

Address all correspondence and requests for reprints to: Goro Katsuura, Department of Medicine and Clinical Science, Kyoto University Graduate School of Medicine, 54 Shougoin Kawahara-cho, Sakyo-ku, Kyoto 606-8507, Japan. E-mail: gorok@kuhp.kyoto-u.ac.jp.

This work was supported in part by research grants from the Ministry of Education, Culture, Sports, Science, and Technology of Japan and by the Ministry of Health, Labor, and Welfare of Japan.

Disclosure Summary: The authors have nothing to disclose.

References

1. Roberts RE, Deleger S, Strawbridge WJ, Kaplan GA 2003 Prospective association between obesity and depression: evidence from the Alameda County Study. Int J Obes Relat Metab Disord 27:514–521
2. Simon GE, Von Korff M, Saunders K, Miglioretti DL, Crane PK, van Belle G, Kessler RC 2006 Association between obesity and psychiatric disorders in the US adult population. Arch Gen Psychiatry 63:824–830
3. Zhao G, Ford ES, Dhingra S, Li C, Strine TW, Mokdad AH 2009 Depression and anxiety among US adults: associations with body mass index. Int J Obes 33:257–266

4. Dong C, Sanchez LE, Price RA 2004 Relationship of obesity to depression: a family-based study. Int J Obes 28:790–795
5. Roberts RE, Strawbridge WJ, Deleger S, Kaplan GA 2002 Are the fat more jolly? Ann Behav Med 24:169–180
6. Myers MG, Cowley MA, Münzberg H 2008 Mechanisms of leptin action and leptin resistance. Annu Rev Physiol 70:537–556
7. Harvey J 2007 Leptin: a diverse regulation of neuronal function. J Neurochem 100:307–313
8. Sahay A, Hen R 2007 Adult hippocampal neurogenesis in depression. Nat Neurosci 10:1110–1115
9. Lu XY, Kim CS, Frazer A, Zhang W 2006 Leptin: a potential novel antidepressant. Proc Natl Acad Sci USA 103:1593–1598
10. Schwartz MW, Peskind E, Raskind M, Boyko EJ, Porter Jr D 1996 Cerebrospinal fluid leptin levels: relationship to plasma levels and to adiposity in humans. Nat Med 2:589–593
11. Hamann A, Matthaei S 1996 Regulation of energy balance by leptin. Exp Clin Endocrinol Diabetes 104:293–300
12. Ogawa Y, Masuzaki H, Hosoda K, Aizawa-Abe M, Suga J, Suda M, Ebihara K, Iwai H, Matsuoka N, Satoh N, Odaka H, Kasuga H, Fujisawa Y, Inoue G, Nishimura H, Yoshimasa Y, Nakao K 1999 Increased glucose metabolism and insulin sensitivity in transgenic skinny mice overexpressing leptin. Diabetes 48:1822–1829
13. Porsolt RD, Bertin A, Jalfre M 1977 Behavioral despair in mice a primary screening test for antidepressants. Arch Int Pharmacodyn Ther 229:327–336
14. Lucki I 1997 The forced swimming test as a model for core and component behavioral effects of antidepressant drugs. Behav Pharmacol 8:523–532
15. Barrot M, Olivier JD, Perrotti LI, DiLeone RJ, Berton O, Eisch AJ, Impey S, Storm DR, Neve RL, Yin JC, Zachariou V, Nestler EJ 2002 CREB activity in the nucleus accumbences shell controls gating of behavioral responses to emotional stimuli. Proc Natl Acad Sci USA 99:11435–11440
16. Willner P 1997 Validity, reliability and utility of the chronic mild stress model of depression: a 10-year review and evaluation. Psychopharmacology 134:319–329
17. Monteggia LM, Luikart B, Barrot M, Theobold D, Malkovska I, Nef S, Parada LF, Nestler EJ 2007 Brain-derived neurotrophic factor conditional knockouts show gender differences in depression-related behaviors. Biol Psychiatry 61:187–197
18. Paxinos G, Franklin KBJ 2004 The mouse brain in stereotaxic coordinates. New York: Academic Press
19. Ebihara K, Ogawa Y, Katsuura G, Numata Y, Masuzaki H, Satoh N, Tamaki M, Yoshioka T, Hayase M, Matsuoka N, Aizawa-Abe M, Yoshimasa Y, Nakao K 1999 Involvement of agouti-related protein, an endogenous antagonist of hypothalamic melanocortin receptor, in leptin action. Diabetes 48:2028–2033
20. Tapley P, Lamballe F, Barbacid M 1992 K252a is a selective inhibitor of the tyrosine protein kinase activity of the trk family of oncogenes and neurotrophin receptors. Oncogene 7:371–381
21. Elias CF, Kelly JF, Lee CE, Ahima RS, Drucker DJ, Saper CB, Elmquist JK 2000 Chemical characterization of leptin-activated neurons in the rat brain. J Comp Neuol 423:261–281
22. Duan W, Guo Z, Mattson MP 2001 Brain-derived neurotrophic factor mediates an excitoprotective effect of dietary restriction in mice. J Neurochem 76:619–626
23. Silhol M, Bonnichon V, Rage F, Tapia-Arancibia L 2005 Age-related changes in brain-derived neurotrophic factor and tyrosine kinase receptor isoforms in the hippocampus and hypothalamus in male rats. Neuroscience 132:613–624
24. Yamada N, Katsuura G, Tatsuno I, Kawahara S, Ebihara K, Saito Y, Nakao K 2009 Orexins increase mRNA expressions of neurotrophin-3 in rat primary cortical neuron cultures. Neurosci Lett 450: 132–135
25. Cohen P, Yang G, Yu X, Soukas AA, Wolfish CS, Friedman JM, Li C 2005 Induction of leptin receptor expression in the liver by leptin and food deprivation. J Biol Chem 280:10034–10039
26. Iwakabe H, Katsuura G, Ishibashi C, Nakanishi S 1997 Impairment of pupillary responses and optokinetic nystagmus in the mGluR6-deficient mouse. Neuropharmacology 36:135–143
27. Considine RV, Sinha MK, Heiman ML, Kriauciunas A, Stephens TW, Nyce MR, Ohannesian JP, Marco CC, McKee LJ, Bauer TL, Caro JF 1996 Serum immunoreactive-leptin concentrations in normal-weight and obese humans. N Engl J Med 334:292–295
28. Nestler EJ, Gould E, Manji H, Buncan M, Duman RS, Gershenfeld HK, Hen R, Koester S, Lederhendler I, Meaney MJ, Robbins T, Winsky L, Zalcman S 2002 Preclinical models: status of basic research in depression. Biol Psychiatry 52:503–528
29. Shirayama Y, Chen AC, Nakagawa S, Russell DS, Duman RS 2002 Brain-derived neurotrophic factor produces antidepressant effects in behavioral models of depression. J Neurosci 22:3251–3261
30. Elmquist JK, Bjørbaek C, Ahima RS, Flier JS, Saper CB 1998 Distributions of leptin receptor mRNA isoforms in the rat brain. J Comp Neurol 395:535–547
31. Mercer JG, Hoggard N, Williams LM, Lawrence CB, Hannah LT, Trayhurn P 1996 Localization of leptin receptor mRNA and the long form splice variant (Ob-Rb) in mouse hypothalamus and adjacent brain regions by in situ hybridization. FEBS Lett 387:113–116
32. Wayner MJ, Armstrong DL, Phelix CF, Oomura Y 2004 Orexin-A (Hypocretin-1) and leptin enhance LTP in the dentate gyrus of rats in vivo. Peptides 25:991–996
33. Farr SA, Banks WA, Morley JE 2006 Effects of leptin on memory processing. Peptides 27:1420–1425
34. O'Malley D, Macdonald N, Mizielinska S, Connolly CN, Irving, AJ, Harvey J 2007 Leptin promotes rapid dynamic changes in hippocampal dendritic morphology. Mol. Cell Neurosci 35:559–572
35. Garza JC, Guo M, Zhang W, Lu XY 2008 Leptin increases adult hippocampal neurogenesis in vivo and in vitro. J Biol Chem 283: 18238–18247
36. Collin M, Håkansson-Ovesjö ML, Misane I, Ogren SO, Meister B 2000 Decreased 5-HT transporter mRNA in neurons of the dorsal raphe nucleus and behavioral depression in the obese leptin-deficient ob/ob mouse. Mol Brain Res 81:51–61
37. Morton GJ, Blevins JE, Williams DL, Niswender KD, Gelling RW, Rhodes CJ, Baskin DG, Schwartz MW 2005 Leptin action in the forebrain regulates the hindbrain response to satiety signals. J Clin Invest 115:703–710
38. Enriori PJ, Evans AE, Sinnayah P, Jobst EE, Tonelli-Lemos L, Billes SK, Glavas MM, Grayson BE, Perello M, Nillni EA, Grove KL, Cowley MA 2007 Diet-induced obesity causes severe but reversible leptin resistance in arcuate melanocortin neurons. Cell Metab 5:181–194
39. Harvey J 2007 Leptin regulation of neuronal excitability and cognitive function. Curr Opin Pharmacol 7:643–647
40. Yamada N, Tatsuno I, Asaki T, Kawahara S, Saito Y, Katsuura G High fat diet-induced obese mice exhibited cognitive impairment in fear conditioning test. Program of the 89th Annual Meeting of the Endocrine Society, Toronto, Canada, 2007 (Abstract OR 30-3)
41. Karege F, Vaudan G, Schwald M, Perroud N, La Harpe R 2005 Neurotrophin levels in postmortem brains of suicide victims and the effects of antemortem diagnosis and psychotropic drugs. Mol Brain Res 136:29–37
42. Martinowich K, Manji H, Lu B 2007 New insights into BDNF function in depression and anxiety. Nat Neurosci 10:1089–1093
43. Pearson S, Schmidt M, Patton G, Dwyer T, Blizzard L, Otahal P, Venn A 2010 Depression and insulin resistance: cross-sectional associations in young adults. Diabetes Care 33:1128–1133
44. Ahola AJ, Thorn LM, Saraheimo M, Forsblom C, Groop PH; Finndiane Study Group 2010 Depression is associated with the metabolic syndrome among patients with type 1 diabetes. Ann Med 42:495–501
45. Robertson SD, Matthies HJ, Owens WA, Sathananthan V, Christianson NS, Kennedy JP, Lindsley CW, Daws LC, Galli A 2010 Insulin reveals Akt signaling as a novel regulator of norepinephrine transporter trafficking and norepinephrine homeostasis. J Neurosci 30:11305–11316

OPEN ACCESS Freely available online PLoS GENETICS

A Mutation in the Gene Encoding Mitochondrial Mg^{2+} Channel MRS2 Results in Demyelination in the Rat

Takashi Kuramoto[1]*, Mitsuru Kuwamura[2], Satoko Tokuda[1,2], Takeshi Izawa[2], Yoshifumi Nakane[1], Kazuhiro Kitada[1,3], Masaharu Akao[4], Jean-Louis Guénet[5], Tadao Serikawa[1]

1 Institute of Laboratory Animals, Graduate School of Medicine, Kyoto University, Kyoto, Japan, **2** Laboratory of Veterinary Pathology, Osaka Prefecture University, Osaka, Japan, **3** Laboratory of Mammalian Genetics, Genome Dynamics Research Center, Graduate School of Science, Hokkaido University, Sapporo, Japan, **4** Department of Cardiovascular Medicine, Graduate School of Medicine, Kyoto University, Kyoto, Japan, **5** Département de Biologie du Développement, Institut Pasteur, Paris, France

Abstract

The rat demyelination (*dmy*) mutation serves as a unique model system to investigate the maintenance of myelin, because it provokes severe myelin breakdown in the central nervous system (CNS) after normal postnatal completion of myelination. Here, we report the molecular characterization of this mutation and discuss the possible pathomechanisms underlying demyelination. By positional cloning, we found that a G-to-A transition, 177 bp downstream of exon 3 of the *Mrs2* (MRS2 magnesium homeostasis factor (*Saccharomyces cerevisiae*)) gene, generated a novel splice acceptor site which resulted in functional inactivation of the mutant allele. Transgenic rescue with wild-type *Mrs2*-cDNA validated our findings. *Mrs2* encodes an essential component of the major Mg^{2+} influx system in mitochondria of yeast as well as human cells. We showed that the *dmy/dmy* rats have major mitochondrial deficits with a markedly elevated lactic acid concentration in the cerebrospinal fluid, a 60% reduction in ATP, and increased numbers of mitochondria in the swollen cytoplasm of oligodendrocytes. MRS2-GFP recombinant BAC transgenic rats showed that MRS2 was dominantly expressed in neurons rather than oligodendrocytes and was ultrastructurally observed in the inner membrane of mitochondria. Our observations led to the conclusion that *dmy/dmy* rats suffer from a mitochondrial disease and that the maintenance of myelin has a different mechanism from its initial production. They also established that Mg^{2+} homeostasis in CNS mitochondria is essential for the maintenance of myelin.

Citation: Kuramoto T, Kuwamura M, Tokuda S, Izawa T, Nakane Y, et al. (2011) A Mutation in the Gene Encoding Mitochondrial Mg^{2+} Channel MRS2 Results in Demyelination in the Rat. PLoS Genet 7(1): e1001262. doi:10.1371/journal.pgen.1001262

Editor: Gregory S. Barsh, Stanford University, United States of America

Received June 5, 2010; **Accepted** November 29, 2010; **Published** January 6, 2011

Funding: This work was supported by grants-in-aid for Scientific Research from the Japan Society for the Promotion of Science [21300153 to TK] and a grant-in-aid for Cancer Research from the Ministry of Health, Labour, and Welfare. The funders had no role in study design, data collection and analysis, decision to publish, or preparation of the manuscript.

Competing Interests: The authors have declared that no competing interests exist.

* E-mail: tkuramot@anim.med.kyoto-u.ac.jp

Introduction

Myelin is an essential component of the nervous tissue of higher vertebrates. It acts as a natural insulator of axonal segments allowing, at the same time, the maintenance of axonal integrity and the fast conduction of action potentials. It also reduces ionic currents across the axonal membrane and stabilizes the extracellular milieu within rapidly-firing axon bundles.

In the central nervous system (CNS), myelin is produced by oligodendrocytes, while in the peripheral nervous system (PNS), this function is achieved by Schwann cells. Myelination is completed within a relatively short period of time during mammalian development and requires a high rate of production and transport of different kinds of molecules, mostly proteins and lipids. In adult life, myelin is constantly remodeled and the maintenance of functional myelin sheaths requires a careful balance of *de novo* synthesis and turnover. It is quite clear that any event generating an imbalance in the myelination or remyelination process has the greatest chance of inducing dys- or demyelination of either the central or peripheral nervous system.

Our knowledge of the myelination process has benefited from careful observations conducted on human patients affected by one of the many defects of myelination or myelin turnover. It has also benefited from researches carried out on animal models, mostly mutant mice and rats, including those that have been induced by transgenesis or genetic engineering in ES cell lines [1,2]. Some of these models have even allowed therapies to be developed in a preclinical setting [3]. Unfortunately, only a small number of the many genes that are directly or indirectly involved in the myelination process have been identified and only a few of these genes have been functionally annotated, for example, by the characterization of one or more mutant alleles. For this reason, any new mutation occurring spontaneously or after mutagenesis is of potential interest for unraveling the molecular mechanisms involved in myelin assembly.

In an earlier paper we reported the discovery and pathology of a rat mutation designated *demyelination* (symbol *dmy*), which is characterized by severe and progressive myelin breakdown in the CNS. We mapped the locus responsible for this myelin disorder to rat chromosome (Chr) 17, very close to the prolactin (*Prl*) locus, in a region homologous to human Chr 6p21.1-22.3 and mouse Chr 13 [4,5]. Based on its pathological features, as well as its genetic localization, this demyelination syndrome appeared to be unique, with no homologue so far reported in any other mammalian species, including humans.

Author Summary

The myelin sheath that surrounds the axon of a neuron acts as a biological insulator. Its major function is to increase the speed at which impulses propagate along myelinated fibers in the central nervous system, as well as the peripheral nervous system. Alterations or damage affecting this structure (demyelination) result in the disruption of signals between the brain and other parts of the body. In the rat, mutations producing demyelination have been frequently identified and characterized and have contributed to a better understanding of the genetics of myelin development, physiology, and pathology. This paper reports the molecular characterization of a recessive allele responsible for the progressive disruption of myelin that was initially observed in mutant rats, previously named demyelination (*dmy*). This mutation generates an additional splicing acceptor site in an intron of the mitochondrial Mg^{2+} transporter gene (*Mrs2*), resulting in the insertion of a 83-bp genomic DNA segment into the *Mrs2* transcript and complete functional inactivation of the mutant allele. We firstly defined the biological function of MRS2 in mammals and demonstrated the crucial and unexpected role of MRS2 in myelin physiology. Our findings might be helpful in the development of new therapeutic strategies for demyelinating syndromes.

In this report we demonstrate that the causative gene (*Mrs2*) encodes a protein that is an essential component of the major electrophoretic Mg^{2+} influx system in mitochondria [6]. This gene has orthologues in other organisms, including lower eukaryotes and plants [7,8]. The protein shares many of the properties of bacterial CorA and yeast Alr1 proteins but its specific involvement in the myelination process was not known or even suspected.

Results

dmy/dmy rats exhibit a phenotype with typical demyelination

The pathology of homozygous *dmy/dmy* rats has been reported in detail previously [4]. Mutant rats exhibit no significant differences from their control littermates until 4 weeks of age. From 5 weeks on, flaccidity of the hind limbs becomes noticeable and evolves towards complete paralysis around 7–8 weeks of age. Progressive demyelination is observed in several parts of the CNS (Figure 1), namely the corpus callosum, the capsula interna, the striatum and the cerebellar peduncle, with major effects on the ventral and lateral parts of the spinal cord. Astrogliosis, which is a major feature of myelin disorder, is observed in demyelinated areas but motor neurons remain normal and there is no sign of associated inflammation in the white matter. The *dmy* mutation can then be regarded as a mutation affecting the maintenance and turnover of myelin rather than its initial production: this is typical demyelination [9].

The *dmy* syndrome is associated with a mutation in a splicing site of *Mrs2*, a gene encoding a mitochondrial Mg^{2+} channel

Out of 687 *dmy/dmy* mutant rats, collected from the 3,252 offspring of an intercross segregating for the *dmy* mutation, 23 individuals were found to carry a recombinant haplotype between the two loci that were used for the initial genetic mapping, namely; *Prl* (prolactin) and *Hh1tts* (testis-specific histone, H1t). Further investigation of these animals, using three novel informative SSLP markers, allowed us to narrow the genetic interval containing *dmy* down to 0.22 cM, between markers *D17Kur17* and *D17Got45*. Within this critical section, we found no recombination between the *dmy* locus and either *Aldh5a1* (aldhehyde dehydrogenase family 5, subfamily A1) or *Mrs2* (mitochondrial 118 RNA splicing2) loci, among $687 \times 2 = 1{,}374$ meioses. The rat genome databases revealed that *D17Kur17* and *D17Got45* were at position 46.78-Mb and 47.26-Mb, respectively, on rat Chr 17, yielding a physical size of 0.48 Mb of DNA for the interval containing the *dmy* locus. This stretch of DNA contained 6 genes (Figure 2A).

Analysis by RT-PCR of the transcription products of these 6 genes revealed that the cDNA transcribed from the *Mrs2* gene was larger in *dmy/dmy* mutants than in the controls (Figure 2B). After sequencing, we found that the larger size of the *dmy* cDNA was due to the insertion of an 83 bp intronic sequence between exons 3 and 4. Comparison of the two genomic sequences revealed a G-to-A transition, 177 bp downstream of the end of exon 3 (Figure 2C, Figure S1), generating a novel splice acceptor site, which accounted for the addition of the 83bp stretch of intronic sequence to the mutant transcript. In addition, while the *Mrs2* gene normally encodes a 434 amino-acid protein, the intronic insertion leads to a shorter protein (106 amino acids) due to the occurrence of a stop codon as a consequence of frame shifting within the novel pseudo-exon X. The new protein consisted of the first 91 amino acids of normal (wild-type) MRS2 protein followed by an additional 15 amino acids transcribed from the intronic stretch (Figure 2D) [10]. No nucleotide alteration was observed between normal and mutant haplotypes in the cDNA transcribed from the other 5 genes (*Vmp*, *Dcdc2*, *Gpld1*, *Aldh5a1*, and *KIAA0319*). These findings strongly suggested that the G-to-A mutation in intron 3 of *Mrs2* in *dmy/dmy* rats was very likely causative of the neurological phenotype.

dmy/dmy rats exhibit morphological and biochemical features characteristic of mitochondrial deficiencies

The MRS2 protein functions as a major transporter protein (Mg^{2+}, Ni^{2+} and Co^{2+}) in yeast as well as in human cells [10,11]. When this protein is functionally defective this leads to the "petite" phenotype in yeast and to cell death in human HEK 293 cells [11,12]. Because mitochondrial diseases in mammals are often accompanied by elevated lactic acid, reduced ATP, increased cytochrome oxidase (COX) activity, and the morphological alteration of mitochondria [13–15], we measured lactic acid levels and ATP contents in the CNS and performed morphological analyses of the CNS of *dmy/dmy* rats.

Lactic acid concentration in the cerebrospinal fluids was significantly elevated in *dmy/dmy* rats when compared with normal littermates: 126 ± 43.7 mg/dL vs 25 ± 9.6 mg/dL (average $\pm$ SD), $P<0.002$ (Figure 3A). The ATP concentration was markedly reduced in *dmy/dmy* rats: 265 ± 79 μM/mg vs 99 ± 46 μM/mg (average $\pm$ SD), $P<0.005$ (Figure 3B). In the affected *dmy/dmy* rats, swollen oligodendrocytes were often observed in the white matter, showing the increased COX reaction products (Figure 3C). Ultrastructurally, their cytoplasm contained many mitochondria and Golgi apparatus-like membrane structures (Figure 3D). These findings indicated that the mitochondria of *dmy/dmy* rats were functionally defective.

Rescue of *dmy/dmy* mutant phenotypes by transgenic complementation

To ascertain that the molecular defect (*i.e.* G-to-A transition) observed in the *dmy* mutant haplotype was causative of the abnormal phenotype observed in *dmy/dmy* rats, we attempted to rescue the mutant phenotype by transgenic complementation. We

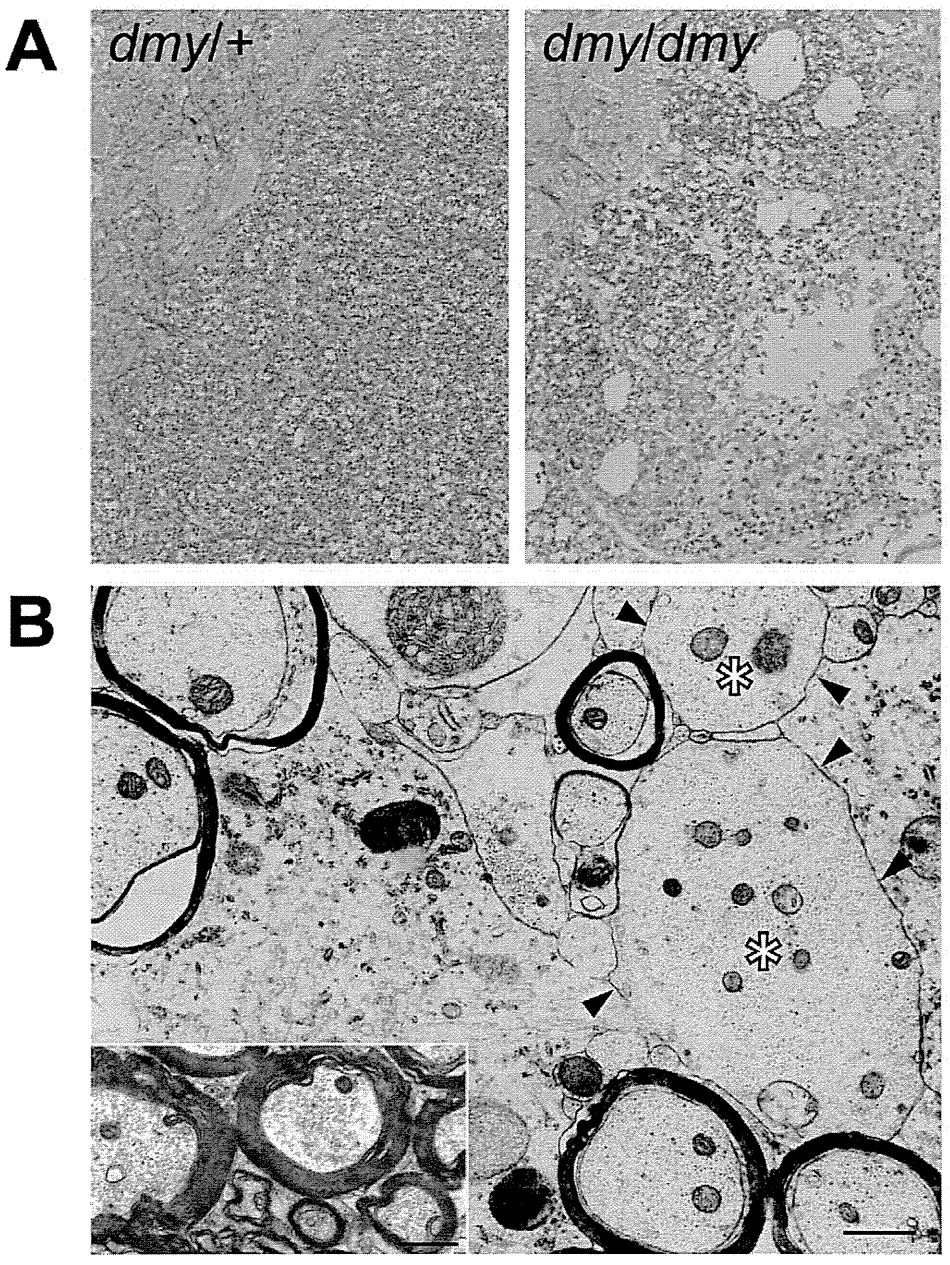

Figure 1. Demyelination in *dmy/dmy* rats. A. Histopathology of the cervical part of the spinal cord of *dmy/+* (left) and *dmy/dmy* (right) rats aged 10 weeks. Luxol fast blue-HE staining. Original magnification: ×100. B. Electron microscopy of the cervical part of spinal cord of *dmy/dmy* rats (10 weeks). Naked axons with demyelination (arrowheads) are indicated by asterisks. Inset: control image of the spinal cord from the age-matched wild type rat. Axons are normally myelinated. Bar = 1 µm.
doi:10.1371/journal.pgen.1001262.g001

established two independent WTC.DMY-*dmy* lines, expressing each *Mrs2* wild-type cDNA under the control of a cytomegalovirus (CMV) promoter (Figure S2A), and found that all *dmy/dmy* transgenic rats exhibited a completely normal phenotype, with no paralysis of the hind limbs. Histopathological analyses demonstrated that both transgenic lines no longer exhibited any sign of demyelination of the CNS (Figure S2B). In addition, lactic acid levels of the cerebrospinal fluid of transgenic *dmy/dmy* rats had returned to the normal range (Figure S2C). Electron microscopic observations revealed that mitochondria of the oligodendrocytes in transgenic rats were normal in their morphology and number (Figure S2D). These findings confirmed that the molecular changes reported above and observed in the *Mrs2* gene were indeed causative of the *dmy*-mutant phenotypes. For this reason we decided that the symbol of the mutant allele should, from now on, be changed to $Mrs2^{dmy}$.

MRS2-GFP recombinant protein is expressed in the mitochondria

To characterize the tissues and cell types expressing MRS2 as well as the subcellular localization of this protein in the CNS, we generated a strain of rats transgenic for a recombinant MRS2-GFP BAC clone. These transgenic rats were expected to express recombinant protein under the control of the endogenous, normal *Mrs2* promoter. We found that cytoplasmic dot-like MRS2-GFP

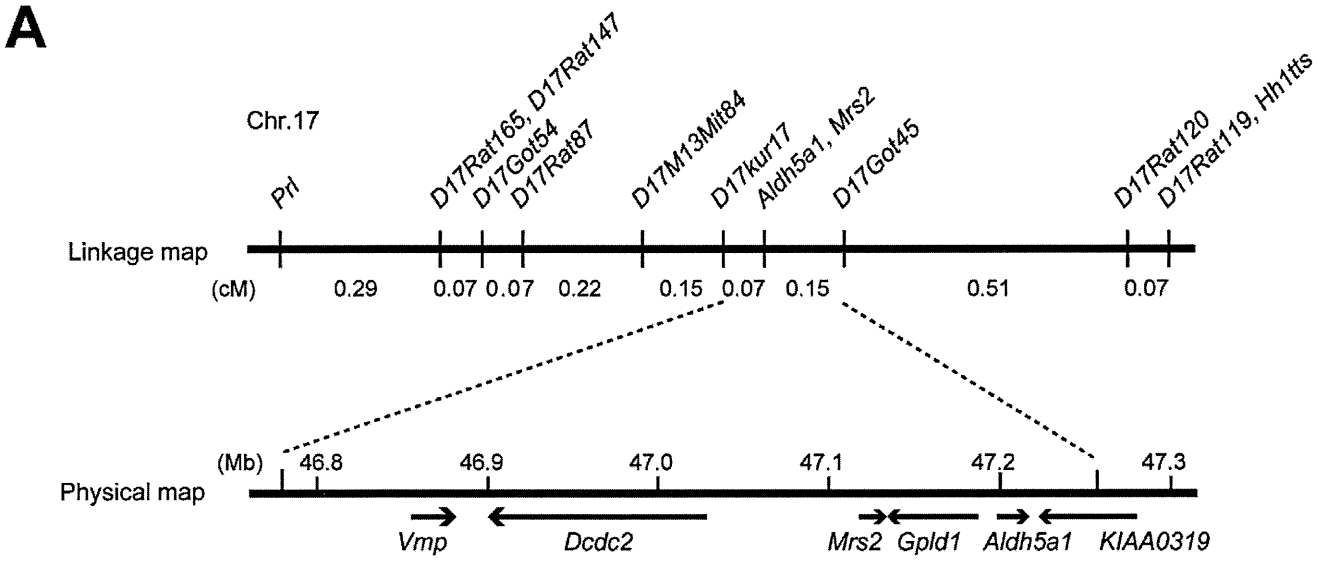
A
Chr.17
Prl
D17Rat165, D17Rat147
D17Got54
D17Rat87
D17M13Mit84
D17kur17
Aldh5a1, Mrs2
D17Got45
D17Rat120
D17Rat119, Hh1tts
Linkage map
(cM)
0.29
0.07
0.07
0.22
0.15
0.07
0.15
0.51
0.07
(Mb)
46.8
46.9
47.0
47.1
47.2
47.3
Physical map
Vmp
Dcdc2
Mrs2
Gpld1
Aldh5a1
KIAA0319

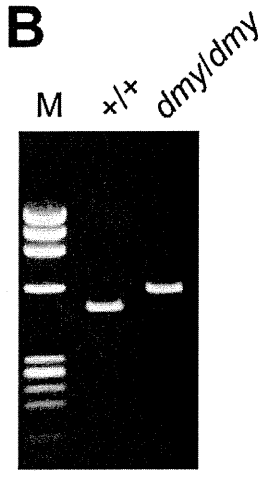
B
M
+/+
dmy/dmy

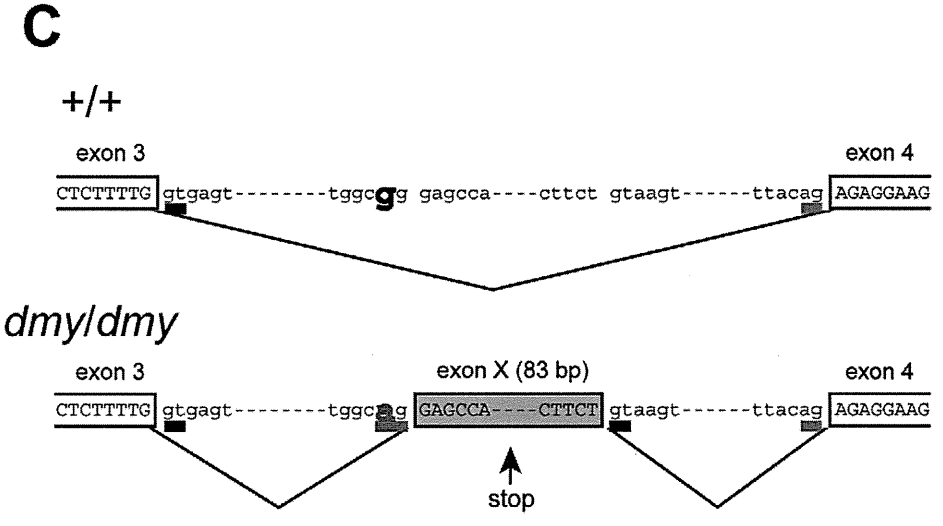
C
+/+
exon 3
exon 4
CTCTTTTG gtgagt--------tggcgg gagcca----cttct gtaagt------ttacag AGAGGAAG
dmy/dmy
exon 3
exon X (83 bp)
exon 4
CTCTTTTG gtgagt--------tggcag GAGCCA----CTTCT gtaagt------ttacag AGAGGAAG
stop

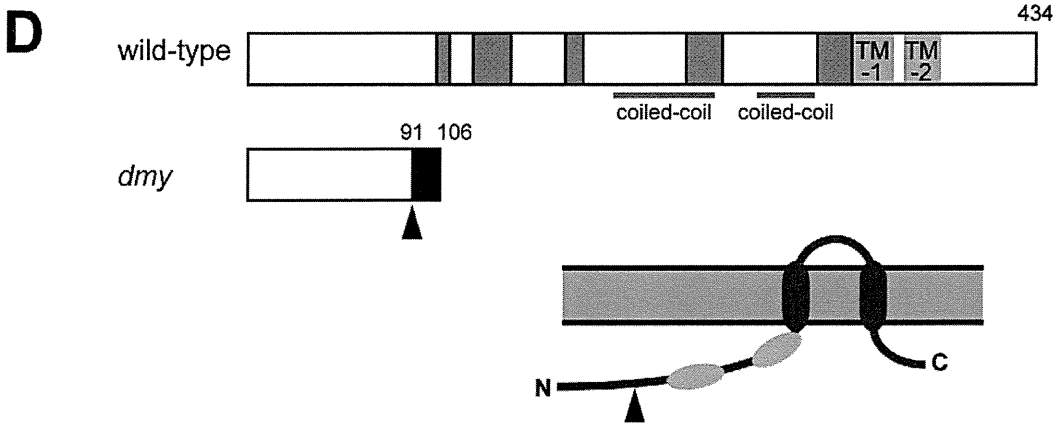
D
wild-type
434
TM -1
TM -2
coiled-coil
coiled-coil
dmy
91 106
N
C

Figure 2. Positional cloning of the *dmy* mutation. A. The *dmy* locus was localized within a 0.22-cM region of chromosome 17 between *D17Kur17* and *D17Got45* and no recombination was observed with SSLP markers designed from *Aldh5a1* and *Mrs2* genomic sequences in 1,374 informative meioses. Within the 0.48-Mb physical interval between *D17Kur17* and *D17Got45*, harboring the *dmy* locus, 6 genes: *Vmp* (vesicular membrane protein p24), *Dcdc2* (doublecortin domain containing 2), *Mrs2* (MRS2 magnesium homeostasis factor (*S. cerevisiae*), *Gpld1* (glycosylphosphatidylinositol specific phospholipase D1), *Aldh5a1* (aldehyde dehydrogenase family 5, subfamily A1), and *KIAA0319*, were previously mapped. B. A larger RT-PCR product was obtained when amplifying the 5′ region of *Mrs2* cDNAs from *dmy/dmy* rats with a primer set of rMrs2l-3&4 (5′-TGTACTGATCTACCCGAGTTCC-3′ and 5′-TCTGGAGTTATCACAGCCTTCA-3′). M: molecular marker, ΦX174-*Hae*III digest. C. Upper: Genomic organization in the vicinity of intron 3 of the *Mrs2* wild-type allele. Lower: Genomic rearrangements in the same intron 3 of the $Mrs2^{dmy}$ mutant allele. In the $Mrs2^{dmy}$ mutant allele, a novel splice acceptor site was generated as a consequence of a G-to-A transition at 177 bp downstream of the end of exon 3. An 83-bp genomic sequence (boxed in gray), downstream of the recently generated acceptor site (tggcag), is then inserted into the *Mrs2* mutant transcript. This sequence contains a premature stop codon (vertical arrow), which truncates the protein almost immediately downstream of exon 3. D. Schematic representations of the wild-type and *dmy* MRS2 proteins. Conserved amino acid residues and transmembrane domains are indicated by grey and purple boxes, respectively. Coiled-coil regions are indicated by horizontal orange lines. The position of the *dmy* mutation is indicated by an arrowhead, and the additional 15 residues (GATWTPRILEECLES), indicated by a black box, are deduced to be added subsequently. Bottom: Schematic representation of the topology of MRS2. Purple: transmembrane domains, Orange: coiled-coil regions. The position of the *dmy* mutation is indicated by an arrowhead.
doi:10.1371/journal.pgen.1001262.g002

signals were observed in neurons throughout the CNS. To a lesser extent, astrocytes and oligodendrocytes also exhibited occasional expression of MRS2 (Figure S3). Confocal microscopy demonstrated that MRS2 is located in the mitochondria (Figure 4A–4C). Moreover, immunoelectron microsopic examinations with anti-GFP antibody revealed that MRS2 is localized in the inner membrane of the mitochondria (Figure 4D). MRS2 expression was also observed in the myocardium, liver, testis and skeletal muscles (Figure S4).

Microglia activation and high expression of inflammatory cytokines were observed in $Mrs2^{dmy}/Mrs2^{dmy}$ rats

Microglial activation, characterized by cellular hypertrophy, has been reported in various dysmyelinating and demyelinating pathologies. To assess microglial activation, we performed immunohistochemistry for IBA1, a specific marker of microglia. In $Mrs2^{dmy}/Mrs2^{dmy}$ rats, prolonged activation of microglia was prominently observed at 6–7 weeks of age (Figure 5A and 5B), the stage at which clinical symptoms such as flaccid paralysis were commonly observed. Expression levels of proinflammatory cytokines, such as *Il1b* and *Il6*, were also significantly higher in $Mrs2^{dmy}/Mrs2^{dmy}$ rats than in wild-type littermates at 6 weeks of age (Figure 5C).

Discussion

Characterization, by positional cloning, of the molecular defect responsible for the demyelinating phenotype observed in adult *dmy/dmy* rats led us to incriminate a mutation in the *Mrs2* gene. No mutant allele before $Mrs2^{dmy}$, which we report here, has ever been reported at this locus in any mammalian species.

Mrs2 encodes an inner membrane Mg^{2+} channel in mitochondria and belongs to a family with orthologous copies in a wide range of species [10,12]. *Mrs2* was originally identified in yeast, and orthologous copies of this gene have been identified in a variety of organisms, including bacteria (CorA), fungi (Alr1), and plants (AtMrs2). All proteins in the family have the same substrate selectivity: they transport Mg^{2+}, Co^{2+} and some other divalent cations across the mitochondrial membrane. Even if these proteins exhibit relatively low sequence similarities, they all have a few important domains at the same relative position and can functionally complement each other over a wide range of phylogenetic distances [16,17]. In mammals, the normal protein MRS2 has two universally conserved transmembrane domains (TMs) and a conserved Gly-Met-Asn (GMN) motif close to the first TM domain that forms part of the pore and is essential for Mg^{2+} transport [18] (Figure 2D, Figure S5). As we demonstrated, the protein is truncated in *dmy/dmy* mutant rats, having lost both of its essential domains and accordingly its function of an Mg^{2+} transmembrane transporter. In other words, $Mrs2^{dmy}$ is a null allele, which is totally consistent with its recessive allelic interaction.

An MRS2 is a major transport for Mg^{2+} uptake into mitochondria, its function would be expected to be important, if not essential, for the maintenance of respiratory complex I and accordingly for cell viability [6,11]. This assumption was supported by the analysis of MRS2 knock-down, mediated by shRNA in a human HEK-293 cell line, which resulted in a series of physiological changes ranging from transient reduction of Mg^{2+} uptake to the complete loss of mitochondrial respiratory complex I, with decreased mitochondrial membrane potential and cell death, depending on the duration of knock-down treatment [11]. However, if we consider the phenotype of our mutant rat, which is apparently limited to the myelination process with a rather long lifespan, the role of MRS2 in the maintenance of cell integrity should be reconsidered.

Considering the pathological features that appear to be characteristics of the $Mrs2^{dmy}$ allele on the one hand, and MRS2-specific functions, as described above on the other, it is logical to consider that the demyelinating syndrome in mutant rats results from a mitochondrial disease. This assertion is supported by the observation of an elevated rate of lactic acid in the cerebrospinal fluid, reduced ATP in the brain, increased COX activity, and the morphological alteration of mitochondria, which is generally considered a major characteristic of mitochondrial diseases [13–15]. An increase in mitochondria is characteristic of cells with reduced respiratory capacity [19]. The association of mitochondrial dysfunction with demyelination (or leukodystrophy) has been already reported in Leigh syndrome and mitochondrial DNA depletion syndrome [20–23]. The tissues most frequently affected in these mitochondrial diseases are the cerebrum, peripheral nerves, and skeletal muscles, presumably because cells of these tissues require more energy than any other cells in the body. Unfortunately, the detailed pathophysiological mechanism(s) leading to demyelination in these diseases has not yet been unraveled. We consider that our mutant rat could be an interesting tool for investigating this matter.

Mitochondrial dysfunction has also been observed in multiple sclerosis (MS), one of the most common demyelination diseases, but here again many aspects of the pathophysiology require further investigation [24,25]. This difficulty of linking gene functions with a specific syndrome is not so surprising if we consider that, according to the most recent estimates, there may be as many as 1,500 nuclear-encoded mitochondrial proteins [26] and that less than half have been identified with experimental support. Clearly, a complete protein inventory of this organelle

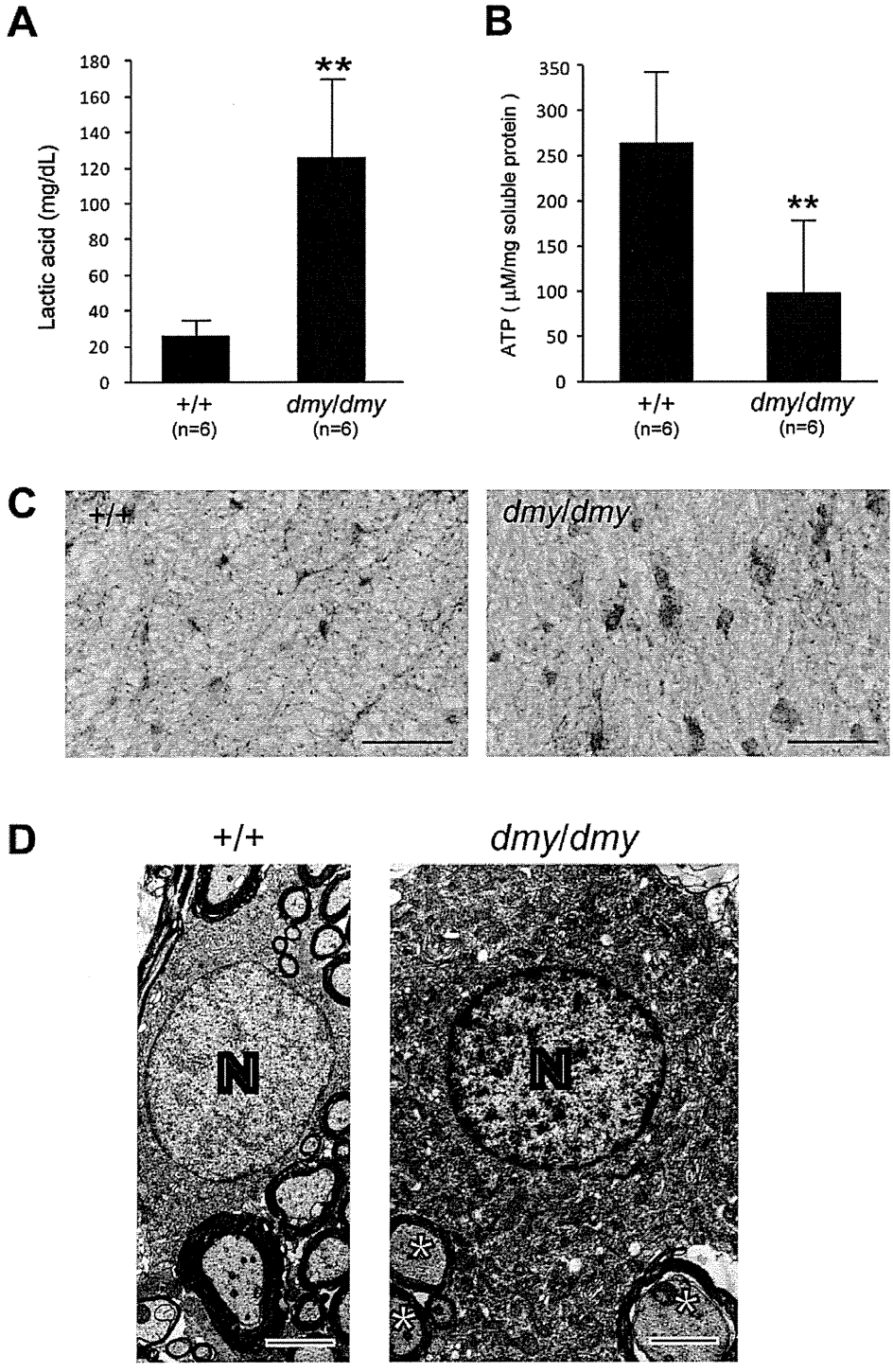

Figure 3. Biochemical and morphological abnormalities in the mitochondria of *dmy/dmy* mutant rats. A. Lactic acid concentration in cerebrospinal fluid of 6–7-week-old *dmy/dmy* rats and age-matched wild-type rats. **, $P<0.002$. B. ATP levels in the brain of 6–7-week-old *dmy/dmy* rats and age-matched wild-type rats. **, $P<0.005$. C. Cytochrome oxidase staining of the spinal cords of 6–7-week-old *dmy/dmy* (right) and age-matched wild-type (left) rats. Swollen oligodendrocytes were often seen they showed increased COX reaction product. Bar = 50 μm. D. Electron microphotographs of a swollen oligodendrocyte in a *dmy/dmy* rat (right) and an oligodendrocyte in a control wild-type rat. White matter of thoracic spine at 6 weeks of age. N: Nucleus of the oligodendrocyte. Axons adjacent to the oligodendrocyte are indicated by asterisks. Bar = 2 μm.
doi:10.1371/journal.pgen.1001262.g003

across tissues would provide a molecular framework to relate mitochondrial biology and pathogenesis [27].

A point concerning *Mrs2* gene expression in the CNS that is worth noting after our experiments and observations is that the gene in question is expressed at a higher rate in neurons than in oligodendrocytes (Figure 4, Figure S3). This was rather unexpected if we consider that oligodendrocytes are the cells actually responsible for myelination of the CNS. At this time, it remains

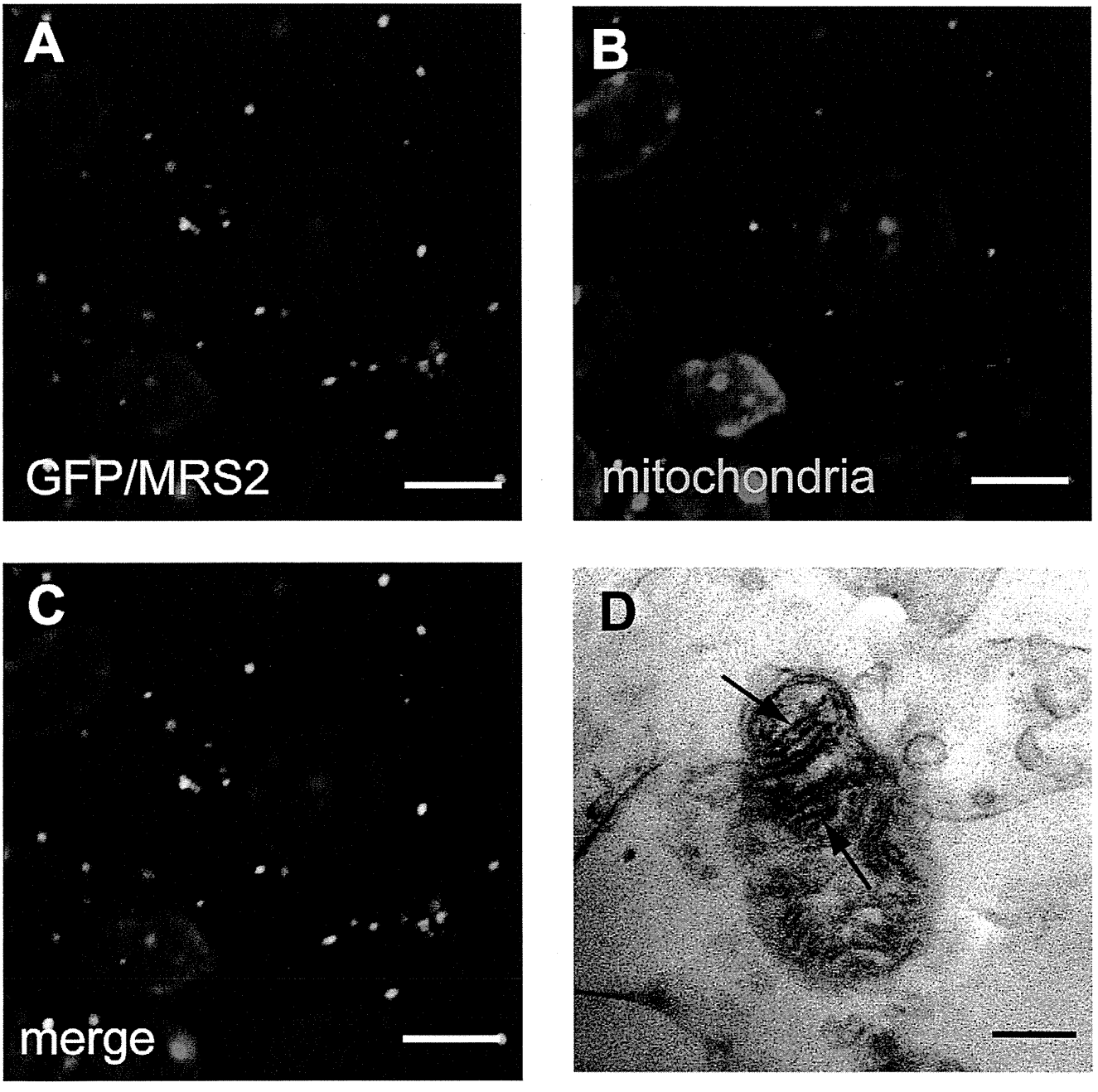

Figure 4. Expression of MRS2 protein in the mitochondria. MRS2-GFP recombinant protein (Green) was seen in the cytoplasm of pyramidal cells (A). MRS2-GFP signals were colocalized with the mitochondria (B), as shown in the confocal image of GFP and mitochondrial immunohistochemistry (C). Nuclei were stained with DAPI (Blue). Bar: 5 μm. Immunoelectron microscopy using anti-GFP antibody revealed that MRS2-GFP signals were localized in the inner membrane of the mitochondria (arrows) (D). Bar: 200 nm.
doi:10.1371/journal.pgen.1001262.g004

unclear whether the demyelination in *dmy/dmy* rats is triggered cell-autonomously or cell-nonautonomously. Instead, it is likely that demyelination is enhanced by the surrounding cells, such as activated microglia and astroglia. At 6 weeks of age, when *dmy/dmy* rats began to exhibit ataxia [9], cytokine levels were elevated and microglia were activated (Figure 5), and it is considered that activated microglia cause neuronal damage through the release of potentially cytotoxic molecules, such as proinflammatory cytokines, reactive oxygen intermediates, proteinases, and complement proteins [28]. Oligodendrocytes show greater vulnerability to such molecules [29,30]. Additionally, Kuwamura and co-workers reported prominent astrogliosis and many ED-1-positive macrophages in myelin-destroyed areas [9]. When considered together, these morphological observations led us to believe that the demyelination observed in *dmy/dmy* rats is probably enhanced by activated microglia and astroglia.

In summary, we identified $Mrs2^{dmy}$ as a loss-of-function mutation of the *Mrs2* gene that normally encodes Mg^{2+} transporter protein of the mitochondrial inner membrane. Our observations also demonstrate that the mechanisms underlying the

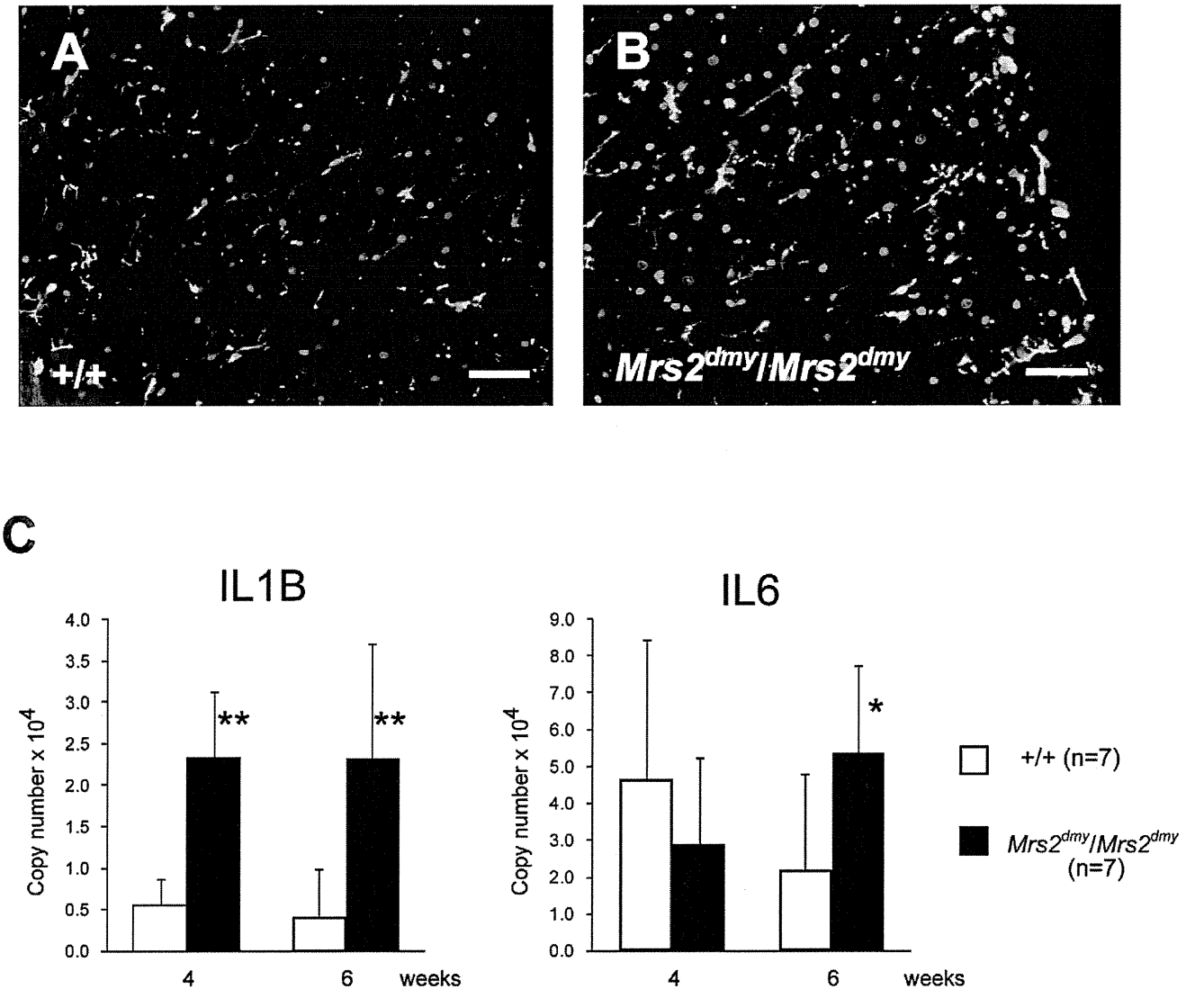

Figure 5. Activation of microglia in the central nervous system of *Mrs2*^{dmy}/*Mrs2*^{dmy} rats. Immunohistochemistry for Iba1 in the lumbar part of the spinal cord of wild-type (A) and *Mrs2*^{dmy}/*Mrs2*^{dmy} rats (B) at 6 weeks of age. Signals of Iba1 (AlexaFluor 546 nm; red), which is upregulated during the activation of microglia, are seen in *Mrs2*^{dmy}/*Mrs2*^{dmy} rats much more the wild-type control. Nucleus is stained with DAPI (blue). C, Inflammatory cytokine mRNA expression in the CNS of wild-type (□) and *Mrs2*^{dmy}/*Mrs2*^{dmy} (■) rats. IL1b expression was elevated in *Mrs2*^{dmy}/*Mrs2*^{dmy} rats at 4 and 6 weeks of age. IL6 was elevated in *Mrs2*^{dmy}/*Mrs2*^{dmy} rats at 6 weeks of age. * $P<0.05$, ** $P<0.005$.
doi:10.1371/journal.pgen.1001262.g005

initial development of myelin (myelination) are different from those that are involved in its maintenance and turnover since, in *Mrs2*^{dmy}/*Mrs2*^{dmy} rats, myelin development is normal while its maintenance is defective. Our mutant rats also appear to be an excellent animal model, not only to evaluate the causal relationships between primary mitochondrial dysfunction and subsequent demyelination, but also for the development of therapies making use, for example, of cell transplantation.

Materials and Methods

Genetic fine mapping of *dmy*

Congenic strains WTC (NBRP#0020) and WTC.DMY-*dmy* (NBRP#0021) were both from the National BioResource Project - Rat, Kyoto University (Kyoto, Japan). (WTC.DMY-*dmy* × BN/SsNSlc)F1(+/*dmy*) rats were intercrossed to produce F2 progeny. *dmy*/*dmy* homozygotes were identified at 7–8 weeks of age, when paralysis of the hind limbs was obvious. 687 *dmy*/*dmy* rats were collected out of 3,252 F2 animals (~21%) and used for fine mapping of the *dmy* locus. Simple sequence length polymorphisms (SSLPs) from the *Prl* (prolactin) and *Hh1tts* (Testis-specific histone, H1t and H4t) genes were used for genotyping as described [31]. To refine the limits of the recombinant interval between *Prl* and *Hh1tts*, two gene-specific and one anonymous SSLP markers were used: *Mrs2* (5′-TCTCCCTTGCCTCTATCTCTCGTCT-3′,5′-CCTGCAGTACTGGGTAAGCCTGATG-3′), *Aldh5a1* (5′-GTTAACTGCACAAGAGCAAGCCAGT-3′, 5′-GCTAATGTTAAGTCATGGGGTGAGG-3′), and *D17Kur17* 5′-ACCTCTTTTTGCCAGCATTG-3′, 5′-CCCTGGGATTGGTCCATA-3′).

All animal experiments were approved by the Animal Research Committee of Kyoto University and were conducted according to the Regulations on Animal Experimentation of Kyoto University.

RT-PCR and direct sequencing

Total RNA was isolated from the brain of 5-week-old animals using ISOGEN (NIPPON GENE, Tokyo, Japan). RT-PCR and direct sequencing of the PCR products were carried out as described previously [32].

Transgenic rescue and recombinant BAC transgenics

A construct containing the CMV promoter, 1.45-kb of the *Mrs2* coding sequence, and SV40 polyA signal was excised from the vector (pCMV-Script; Agilent Technologies, CA, USA) and used as a transgene, which was microinjected into the pronuclei of fertilized oocytes collected from Crj:Wistar rats. Transgenic offspring founder rats were then crossed with WTC- +/*dmy* rats and then backcrossed again to WTC- +/*dmy* rats to obtain *dmy*/*dmy* homozygous and also hemizygous for the transgene (*dmy*/*dmy*, tg/-). Expression of the transgene was confirmed by RT-PCR with primers (5′-GCGAATGGAGATCCAATTTT-3′, 5′-GGGAGGTGTGGGAGGTTTT-3′) to detect SV40 polyA sequence. Brain RNA was treated with DNase I (New England BioLabs) to remove contaminating genomic DNA and then subjected to cDNA synthesis.

A rat BAC clone, CHORI-230-9K13, including the rat *Mrs2* gene was modified to express MR2SL-EGFP fusion protein under the endogenous promoter by ET recombination technology [33]. Modified genomic DNA was excised from the vector and then used for *in ovo* transgenesis.

Quantitative PCR

Real-time PCR was performed using the Thermal Cycler Dice Real Time System (Takara Bio Inc., Otsu, Japan) with SYBR Premix Ex Taq II (Takara Bio Inc., Otsu, Japan). By monitoring amplification curves of a test sample and reference samples that contained 101–106 molecules of the gene of interest, the number of target molecules in the test sample was analyzed. The number of target molecules was normalized to that of glyceraldehyde-3-phosphate dehydrogenase (*Gapdh*) as an internal control. The primers used are as follows: 5′-GCTGTGGCAGCTACCTATGTCTTG-3′ and 5′-AGGTCGTCATCATCCCACGAG-3′ for the rat Interleukin-1b (*Il1b*), 5′-CCACTTCACAAGTCGGAGGCTTA-3′ and 5′-GTGCATCATCGCTGTTCATACAATC-3′ for the rat interleukin-6 (*Il6*), 5′-GGCACAGTCAAGGCTGAGAATG-3′ and 5′-ATGGTGGTGAAGACGCCAGTA-3′ for rat *Gapdh*.

Electron microscopy

Perfusion fixation through the left ventricle was conducted with 4% paraformaldehyde in 0.1 M phosphate buffer (PB). Brains and spinal cords were dissected and stored in 2% paraformaldehyde and 2.5% glutaraldehyde in 0.1 M PB, then post-fixed with 2% osmic acid for 2 hours and embedded in epoxy resin. Ultrathin sections were double-stained with uranyl acetate and lead citrate and examined by a Hitachi H-7500 electron microscope (Hitachi, Tokyo, Japan).

Immunohistochemistry

Immunohistochemistry was performed as described previously [9]. The following primary antibodies were used: monoclonal anti-2′, 3′-cyclic nucleotide-3′-phosphodiesterase (CNPase) for oligodendrocytes (1:1,000; Sigma, St. Louis, MO, USA), monoclonal anti-mitochondria (1:100; Abcam, Cambridge, MA, USA), polyclonal anti-GFAP for astrocytes (1:1,000; Dako, Carpinteria, CA, USA), polyclonal anti-Iba1 for microglia/macrophages (1:200; Wako Pure Chemical Industries, Osaka, Japan). Cy3-conjugated anti-mouse IgG (1:500; Jackson Laboratories) or Alexa 588-conjugated anti-rabbit IgG (1:500; Molecular Probes) antibody was reacted. Nuclei were counterstained with DAPI (Vactor Laboratories). Signals were detected with a fluorescence microscopy (Olympus, Tokyo, Japan) or a confocal imaging system (C1Si; Nikon, Tokyo, Japan).

For immunoelectron microscopy, PFA-perfused frozen sections were incubated with rabbit antibody against fluorescent protein (1:2,000; Molecular Probes) at 4 °C overnight. After washing in PBS, peroxidase-conjugated anti-rabbit IgG Fab fraction (Jackson Laboratories, 1:1,000) and immunoreactions were reacted 3,3-diaminobenzidine substrate kit (Vector Laboratories), postfixed in 1% osmium tetraoxide, dehydrated in graded ethanol, and then embedded in epoxy resin. Ultrathin sections were examined by electron microscopy (Hitachi, Tokyo, Japan).

Lactic acid measurements

Cerebrospinal fluid was collected from *dmy*/*dmy*, wild-type littermates, and *dmy*/*dmy* with the normal *Mrs2* transgene at 6–7 weeks of age under isoflurane anesthesia. They were then mixed with 0.8N perchloric acid to inactivate proteins. After centrifugation, lactic acid concentrations of the supernatants were measured by Determiner LA (KYOWA MEDEX Co., Ltd., Tokyo, Japan).

Cytochrome oxidase histochemistry

Frozen spinal cord sections were prepared. Then, 100 µl of freshly prepared reaction buffer [50 mM Tris/HCl (pH 7.4), 0.5 mg/ml diaminobenzidine, 20 µg/ml catalase and 0.50 mg/ml cytochrome C] was added to each section and slides were incubated for 30 min at 37°C.

ATP measurements

Rats were sacrificed by cervical dislocation and the brains were immediately excised, frozen in liquid nitrogen, and stored at −80°C until measurement. In order to release cellular ATP, frozen tissue (25 mg) was boiled for 2 min after the addition of 300 µl water containing 100 mM Tris/HCl (pH 7.75) and 4 mM EDTA. Samples were placed on ice and homogenized by sonification (micro tip, 1 s ×10 pulse). ATP concentrations were determined using the ATP bioluminescence assay kit HS II (Roche) according to the manufacturer's protocol. Data were standardized to the protein concentration which was determined by Coomassie Plus – the better Bradford assay kit (Pierce).

Statistical analysis

Statistical differences in lactic acid, ATP and mRNA expressions between wild-type and *dmy*/*dmy* rats were evaluated using the Mann-Whitney U test.

Supporting Information

Figure S1 Detection of the $Mrs2^{dmy}$ mutation. A. Chromatograms showing the $Mrs2^{dmy}$ G-to-A mutation. Upper: wild-type genome. Lower: $Mrs2^{dmy}/Mrs2^{dmy}$ genome. The $Mrs2^{dmy}$ mutation disrupted *Aci*I restriction site (GGCG) in the $Mrs2^{dmy}/Mrs2^{dmy}$ genome. B. Molecular diagnosis of the $Mrs2^{dmy}$ mutation. In the wild type, the 349-bp PCR product amplified with primers rMrs2-31&32 (5′-AAAGTTTGACAAAGAAGGAAACG-3′ and 5′-GGGGATGGAGGGCTATGTAA-3′) is digested with *Aci*I but not in $Mrs2^{dmy}/Mrs2^{dmy}$ mutant rats. M: ΦX174-*Hae*III digests.
Found at: doi:10.1371/journal.pgen.1001262.s001 (1.15 MB TIF)

Figure S2 Transgenic rescue experiment. A. Expression of the transgene in the brain of a transgenic rat. Brain cDNA from Tg-

positive rats (Lanes 2 and 3) and Tg-negetive rats (Lanes 1and 4) was used as templates. Brain RNA was treated with DNaseI to remove contaminating genomic DNA. M: ΦX174 *Hae*III digests. B. Histopathology of the cervical part of the spinal cord of *dmy/dmy* transgene-negative rats (left) and *dmy/dmy* transgene-positive (right) rats aged 10 weeks. Luxol fast blue-HE staining. Original magnification: ×100. C. Lactic acid concentration in cerebrospinal fluid of 6-7-week-old *dmy/dmy* rats and age-matched *dmy/dmy Mrs2* cDNA-transgenic rats. Elevated lactic acid (126 ± 43.7 mg/dL) was reduced to normal level (22 ± 3.1 mg/dL). **, $P < 0.002$. D. Electron microphotograph of an oligodendrocyte in a *dmy/dmy* transgene-positive rat. Densely packed mitochondria (arrowheads) were found in the cytoplasm. Bar: 2μm.
Found at: doi:10.1371/journal.pgen.1001262.s002 (5.52 MB TIF)

Figure S3 MRS2 expression in the CNS of Mrs2-GFP recombinant BAC transgenic rats. MRS2 signals were mainly found in neurons (A), and occasionally in GFAP-positive astrocytes (B) and CNP-positive oligodendrocytes (C). Left: Bar: 50 μm. Center, Right: Bar: 20 μm.
Found at: doi:10.1371/journal.pgen.1001262.s003 (3.15 MB TIF)

Figure S4 MRS2 expression in Mrs2-GFP recombinant BAC transgenic rats. MRS2 signals were observed in the myocardium (A), liver (B), testis (C) and skeletal muscles (D). Bar: 50 μm.
Found at: doi:10.1371/journal.pgen.1001262.s004 (6.29 MB TIF)

Figure S5 Sequence alignment of yeast, human, and rat MRS2 proteins. Predicted transmembrane domains (TM-1, TM-2) are boxed; * indicates identical residues; : indicates conservative substitution; . indicates semiconservative substitutions. The sequence of a motif conserved in all putative magnesium transporters, G-M-N, is indicated in bold. Predicted coiled-coil regions are underlined, five regions with conserved amino acid residues (CRB-1-5; conserved residue block) are shaded grey. Arrowhead: The position of the residue affected by the *dmy* mutation, after which the 15 additional residues follow in mutant MRS2.
Found at: doi:10.1371/journal.pgen.1001262.s005 (1.38 MB TIF)

Acknowledgments

The authors are grateful to M. Yokoe for excellent technical assistance.

Author Contributions

Conceived and designed the experiments: TK. Performed the experiments: TK MK ST TI YN KK. Analyzed the data: TK MK. Contributed reagents/materials/analysis tools: MA TS. Wrote the paper: TK MK JLG.

References

1. Werner H, Jung M, Klugmann M, Sereda M, Griffiths IR, et al. (1998) Mouse models of myelin diseases. Brain Pathol 8: 771–793.
2. Griffiths IR (1996) Myelin mutants: model systems for the study of normal and abnormal myelination. Bioessays 18: 789–797.
3. Meyer Zu Horste G, Nave KA (2006) Animal models of inherited neuropathies. Curr Opin Neurol 19: 464–473.
4. Kuramoto T, Sotelo C, Yokoi N, Serikawa T, Gonalons Sintes E, et al. (1996) A rat mutation producing demyelination (*dmy*) maps to chromosome 17. Mamm Genome 7: 890–894.
5. Kitada K, Guenet JL, Serikawa T (2000) Determination of the mouse homologous region for the rat *dmy* locus. J Exp Anim Sci 41: 40–43.
6. Schindl R, Weghuber J, Romanin C, Schweyen RJ (2007) Mrs2p forms a high conductance Mg^{2+} selective channel in mitochondria. Biophys J 93: 3872–3883.
7. Gregan J, Bui DM, Pillich R, Fink M, Zsurka G, et al. (2001) The mitochondrial inner membrane protein Lpe10p, a homologue of Mrs2p, is essential for magnesium homeostasis and group II intron splicing in yeast. Mol Gen Genet 264: 773–781.
8. Schock I, Gregan J, Steinhauser S, Schweyen R, Brennicke A, et al. (2000) A member of a novel Arabidopsis thaliana gene family of candidate Mg^{2+} ion transporters complements a yeast mitochondrial group II intron-splicing mutant. Plant J 24: 489–501.
9. Kuwamura M, Kanehara T, Tokuda S, Kumagai D, Yamate J, et al. (2004) Immunohistochemical and morphometrical studies on myelin breakdown in the demyelination (*dmy*) mutant rat. Brain Res 1022: 110–116.
10. Kolisek M, Zsurka G, Samaj J, Weghuber J, Schweyen RJ, et al. (2003) Mrs2p is an essential component of the major electrophoretic Mg^{2+} influx system in mitochondria. Embo J 22: 1235–1244.
11. Piskacek M, Zotova L, Zsurka G, Schweyen RJ (2009) Conditional knockdown of hMRS2 results in loss of mitochondrial Mg^{2+} uptake and cell death. J Cell Mol Med 13: 693–700.
12. Wiesenberger G, Waldherr M, Schweyen RJ (1992) The nuclear gene MRS2 is essential for the excision of group II introns from yeast mitochondrial transcripts in vivo. J Biol Chem 267: 6963–6969.
13. Devivo DC (1993) The expanding clinical spectrum of mitochondrial diseases. Brain Dev 15: 1–22.
14. Huttemann M, Zhang Z, Mullins C, Bessert D, Lee I, et al. (2009) Different proteolipid protein mutants exhibit unique metabolic defects. ASN Neuro 1.
15. Thambisetty M, Newman NJ (2004) Diagnosis and management of MELAS. Expert Rev Mol Diagn 4: 631–644.
16. Bui DM, Gregan J, Jarosch E, Ragnini A, Schweyen RJ (1999) The bacterial magnesium transporter CorA can functionally substitute for its putative homologue Mrs2p in the yeast inner mitochondrial membrane. J Biol Chem 274: 20438–20443.
17. Zsurka G, Gregan J, Schweyen RJ (2001) The human mitochondrial Mrs2 protein functionally substitutes for its yeast homologue, a candidate magnesium transporter. Genomics 72: 158–168.
18. Eshaghi S, Niegowski D, Kohl A, Martinez Molina D, Lesley SA, et al. (2006) Crystal structure of a divalent metal ion transporter CorA at 2.9 angstrom resolution. Science 313: 354–357.
19. Detmer SA, Chan DC (2007) Functions and dysfunctions of mitochondrial dynamics. Nat Rev Mol Cell Biol 8: 870–879.
20. Hung PC, Wang HS (2007) A previously undescribed leukodystrophy in Leigh syndrome associated with T9176C mutation of the mitochondrial ATPase 6 gene. Dev Med Child Neurol 49: 65–67.
21. Navarro-Sastre A, Martin-Hernandez E, Campos Y, Quintana E, Medina E, et al. (2008) Lethal hepatopathy and leukodystrophy caused by a novel mutation in MPV17 gene: description of an alternative MPV17 spliced form. Mol Genet Metab 94: 234–239.
22. Spinazzola A, Viscomi C, Fernandez-Vizarra E, Carrara F, D'Adamo P, et al. (2006) MPV17 encodes an inner mitochondrial membrane protein and is mutated in infantile hepatic mitochondrial DNA depletion. Nat Genet 38: 570–575.
23. Zafeiriou DI, Koletzko B, Mueller-Felber W, Paetzke I, Kueffer G, et al. (1995) Deficiency in complex IV (cytochrome c oxidase) of the respiratory chain, presenting as a leukodystrophy in two siblings with Leigh syndrome. Brain Dev 17: 117–121.
24. Andrews HE, Nichols PP, Bates D, Turnbull DM (2005) Mitochondrial dysfunction plays a key role in progressive axonal loss in Multiple Sclerosis. Med Hypotheses 64: 669–677.
25. Mahad DJ, Ziabreva I, Campbell G, Lax N, White K, et al. (2009) Mitochondrial changes within axons in multiple sclerosis. Brain 132: 1161–1174.
26. Lopez MF, Kristal BS, Chernokalskaya E, Lazarev A, Shestopalov AI, et al. (2000) High-throughput profiling of the mitochondrial proteome using affinity fractionation and automation. Electrophoresis 21: 3427–3440.
27. Pagliarini DJ, Calvo SE, Chang B, Sheth SA, Vafai SB, et al. (2008) A mitochondrial protein compendium elucidates complex I disease biology. Cell 134: 112–123.
28. Dheen ST, Kaur C, Ling EA (2007) Microglial activation and its implications in the brain diseases. Curr Med Chem 14: 1189–1197.
29. Merrill JE, Scolding NJ (1999) Mechanisms of damage to myelin and oligodendrocytes and their relevance to disease. Neuropathol Appl Neurobiol 25: 435–458.
30. Mitrovic B, Ignarro LJ, Montestruque S, Smoll A, Merrill JE (1994) Nitric oxide as a potential pathological mechanism in demyelination: Its differential effects on primary glial cells in vitro. Neuroscience 61: 575–585.
31. Serikawa T, Kuramoto T, Hilbert P, Mori M, Yamada J, et al. (1992) Rat gene mapping using PCR-analyzed microsatellites. Genetics 131: 701–721.
32. Kuramoto T, Kitada K, Inui T, Sasaki Y, Ito K, et al. (2001) Attractin/mahogany/zitter plays a critical role in myelination of the central nervous system. Proc Natl Acad Sci U S A 98: 559–564.
33. Zhang Y, Buchholz F, Muyrers JP, Stewart AF (1998) A new logic for DNA engineering using recombination in *Escherichia coli*. Nat Genet 20: 123–128.

http://www.kidney-international.org

Pleiotrophin triggers inflammation and increased peritoneal permeability leading to peritoneal fibrosis

Hideki Yokoi[1,2], Masato Kasahara[1,2], Kiyoshi Mori[1], Yoshihisa Ogawa[1], Takashige Kuwabara[1], Hirotaka Imamaki[1], Tomoko Kawanishi[1], Kenichi Koga[1], Akira Ishii[1], Yukiko Kato[1], Keita P. Mori[1], Naohiro Toda[1], Shoko Ohno[1], Hisako Muramatsu[3], Takashi Muramatsu[4], Akira Sugawara[1], Masashi Mukoyama[1] and Kazuwa Nakao[1]

[1]Department of Medicine and Clinical Science, Kyoto University Graduate School of Medicine, Kyoto, Japan; [2]Division of Nephrology and Blood Purification, Kobe Institute of Biomedical Research and Innovation, Hyogo, Japan; [3]Department of Health and Nutrition, Faculty of Psychological and Physical Science, Aichi Gakuin University, Aichi, Japan and [4]Department of Health Science, Faculty of Psychological and Physical Science, Aichi Gakuin University, Aichi, Japan

Long-term peritoneal dialysis induces peritoneal fibrosis with submesothelial fibrotic tissue. Although angiogenesis and inflammatory mediators are involved in peritoneal fibrosis, precise molecular mechanisms are undefined. To study this, we used microarray analysis and compared gene expression profiles of the peritoneum in control and chlorhexidine gluconate (CG)-induced peritoneal fibrosis mice. One of the 43 highly upregulated genes was pleiotrophin, a midkine family member, the expression of which was also upregulated by the solution used to treat mice by peritoneal dialysis. This growth factor was found in fibroblasts and mesothelial cells within the underlying submesothelial compact zones of mice, and in human peritoneal biopsy samples and peritoneal dialysate effluent. Recombinant pleiotrophin stimulated mitogenesis and migration of mouse mesothelial cells in culture. We found that in wild-type mice, CG treatment increased peritoneal permeability (measured by equilibration), increased mRNA expression of TGF-β1, connective tissue growth factor and fibronectin, TNF-α and IL-1β expression, and resulted in infiltration of CD3-positive T cells, and caused a high number of Ki-67-positive proliferating cells. All of these parameters were decreased in peritoneal tissues of CG-treated pleiotrophin-knockout mice. Thus, an upregulation of pleiotrophin appears to play a role in fibrosis and inflammation during peritoneal injury.

Kidney International (2012) **81,** 160–169; doi:10.1038/ki.2011.305; published online 31 August 2011

KEYWORDS: continuous ambulatory peritoneal dialysis; microarray analysis; peritoneal dialysis; peritoneal membrane

Correspondence: *Masato Kasahara, Department of Medicine and Clinical Science, Kyoto University Graduate School of Medicine, 54 Shogoin Kawahara-cho, Sakyo-ku, Kyoto 606-8507, Japan.*
E-mail: kasa@kuhp.kyoto-u.ac.jp

Received 8 December 2010; revised 19 June 2011; accepted 5 July 2011; published online 31 August 2011

Continuous ambulatory peritoneal dialysis (PD) is a preferred method of home dialysis for patients with end-stage renal failure.[1] Long-term use of PD induces peritoneal fibrosis characterized with the presence of submesothelial fibrotic tissue and increased peritoneal vascularization with vasculopathy.[2] Peritoneal fibrosis occurs in long-term continuous ambulatory PD patients in response to a variety of injuries, including bioincompatible dialysate solutions, peritonitis, uremia, and chronic inflammation.[2,3] Previous reports show that several profibrotic and proinflammatory mediators are upregulated upon induction of peritoneal fibrosis, such as transforming growth factor-β (TGF-β) and interleukin-6 (IL-6).[4–6] Although proinflammatory, angiogenic, and profibrotic cytokines such as IL-1β, vascular endothelial growth factor, and TGF-β are presumed to be involved in the pathogenesis, precise molecular mechanisms that lead to peritoneal sclerosis and encapsulating peritoneal sclerosis are still elusive.[7–9] To identify the novel genes possibly involved in the development of peritoneal fibrosis, we compared gene expression profiles of the peritoneum in chlorhexidine gluconate (CG)-induced peritoneal fibrosis and control mice using microarray.

Microarray analysis is a powerful tool to identify novel genes and pathways involved in the development of peritoneal fibrosis. Although a few papers report microarray analysis for endothelial cells in rat peritoneal dialysate infusion model,[10] analysis for whole mouse gene sets over 39,000 transcripts has not been investigated yet. In this study, we performed microarray analysis using a mouse model of peritoneal fibrosis and selected the genes that changed greatly in peritoneal fibrosis and those that were also present in mesothelial cells. This approach can allow us to specify the genes associated with peritoneal injury.

Here we show that one of the highly upregulated secreted proteins during the development of peritoneal fibrosis is pleiotrophin (PTN). PTN is an 18-kDa secreted protein, belonging to the midkine family and has functions similar to

midkine.[11] The receptors for PTN are the receptor protein tyrosine phosphatase β/ζ (RPTPβ/ζ), anaplastic lymphoma tyrosine kinase (ALK), and syndecan-3.[12] PTN has been shown to promote cell growth, migration, oncogenesis, and angiogenesis.[11] However, the role of PTN in peritoneal fibrosis remains unknown. To elucidate the role of PTN in peritoneal injury, we examined the PTN expression in a mouse model of peritoneal fibrosis and in human peritoneal biopsy samples. We also investigated the functional significance of PTN by using PTN-deficient mice.[13]

RESULTS

To screen novel genes involved in development of peritoneal fibrosis, we compared the gene expression profiles between phosphate buffered saline (PBS)-injected and CG-injected mice three times a week for 3 weeks. As a control, PBS-injected wild-type mice showed no peritoneal fibrosis. CG-injected mice showed marked thickened submesothelial peritoneal membrane compared with PBS-injected mice (Figure 1a, CG-injected mice: 228 μm vs. PBS-injected mice: 34 μm). We performed microarray analysis using parietal peritoneum in mice at 21 days after PBS and CG treatment. We identified genes differentially expressed between PBS- and CG-injected mice, which were also expressed in murine cultured mesothelial cells. Table 1 shows one downregulated and 43 upregulated genes that were expressed by eightfold or greater in CG-treated mice than that in PBS-treated wild-type mice, and which were expressed in the cultured mesothelial

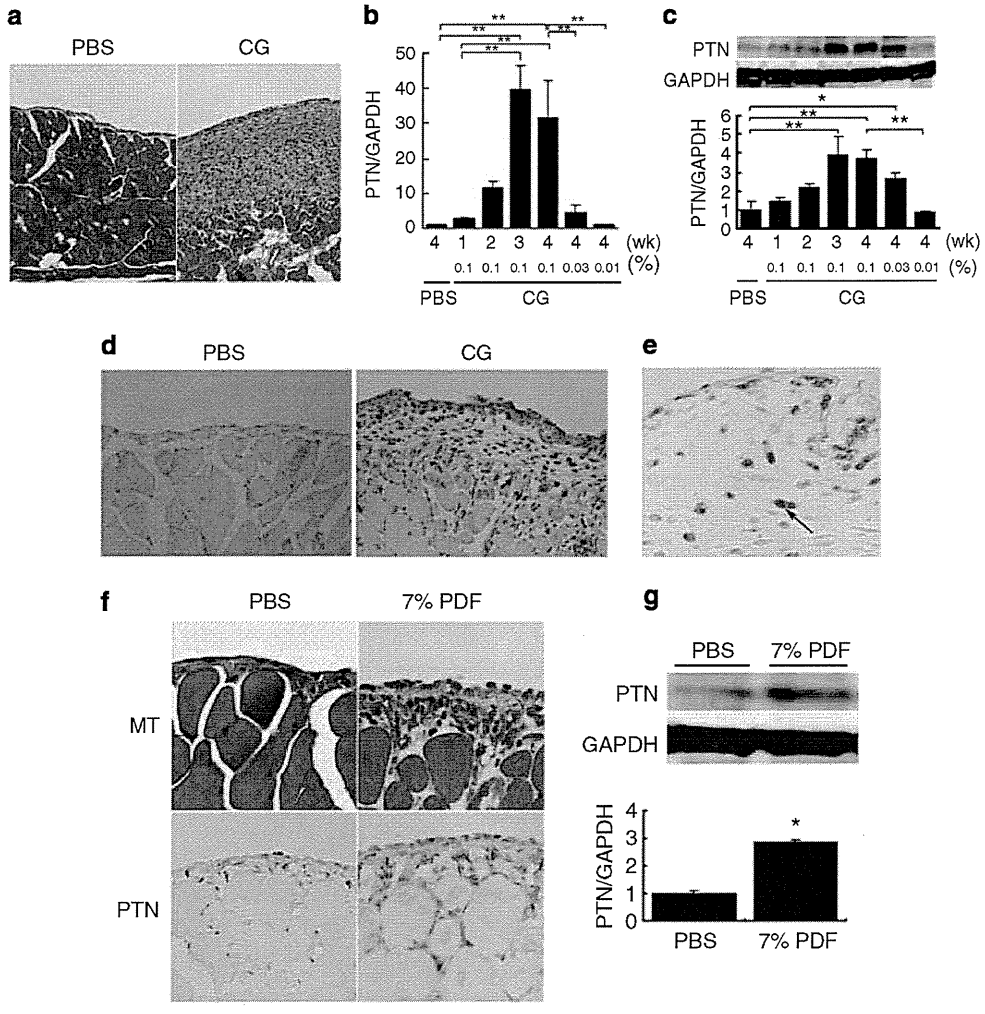

Figure 1 | PTN expression in a mouse model of peritoneal fibrosis. (**a**) Microscopic examination of peritoneal fibrosis model mice. C57BL/6J wild-type mice (WT) treated with phosphate-buffered saline (PBS) showed no fibrosis in the peritoneum. Chlorhexidine gluconate (CG)-treated mice exhibited marked peritoneal fibrosis with moderate infiltration of mononuclear cells on day 21 ($n = 3$, each, original magnification × 20). Pleiotrophin (PTN) mRNA expression (**b**) or protein (**c**) in the peritoneum of PBS- or CG-treated mice was analyzed by real-time reverse transcriptase-polymerase chain reaction analysis or western blot analysis, respectively. GAPDH was used as internal control ($n = 5$, each). (**d**) Immunohistochemical study for PTN (brown). Mesothelial cells and the cells in submesothelial layer were positive for PTN. (**e**) Double immunohistochemical study for PTN (brown) and S100A4 (blue). Some of PTN-positive cells were also positive for S100A4 (arrow). (**f**) Mice receiving daily intraperitoneal injection of 7% peritoneal dialysis fluid (PDF) for 4 weeks showed increased submesothelial layer thickness by Masson's trichrome staining (MT) and upregulated PTN protein in the submesothelial layer ($n = 5$, each). (**g**) Western blot analysis showed that PTN protein in PDF-treated mice was 1.9 times higher than the control. GAPDH was used as internal control. Mean ± s.e. $^*P < 0.05$, $^{**}P < 0.01$ vs. PBS. GAPDH, glyceraldehyde-3-phosphate dehydrogenase; wk, week.

Table 1 | Genes changed in parietal peritoneum in chlorhexidine gluconate (CG)-treated mice compared with phosphate-buffered saline-treated mice after 3 weeks of CG treatment and in the presence of cultured mesothelial cells

Gene title	ID	Fold change of gene up- or downregulated in CG-treated mice compared with PBS-treated mice	Gene symbol
Glucocortoid-regulated inflammatory prostaglandin GH synthase (griPGHS)	M94967	168.897	*Ptgs2*
Procollagen, type VIII, alpha 1	NM_007739	73.51669	*Col8a1*
DEAD (Asp-Glu-Ala-Asp) box polypeptide 3, Y-linked	AA210261	55.71524	*Ddx3y*
Eukaryotic translation initiation factor 2, subunit 3, structural gene Y-linked	NM_012011	48.50293	*Eif2s3y*
A disintegrin and metallopeptidase domain 12 (meltrin alpha)	NM_007400	42.22425	*Adam12*
Interleukin 6	NM_031168	25.99208	*Il6*
Chemokine (C-X-C motif) ligand 1	NM_008176	24.25147	*Cxcl1*
Matrix metallopeptidase 14 (membrane-inserted)	NM_008608	24.25147	*Mmp14*
Chemokine (C-C motif) ligand 7	AF128193	17.14838	*Ccl7*
Ankyrin repeat domain 1 (cardiac muscle)	AK009959	16	*Ankrd1*
Leucine-rich repeat containing 15	AK017350	14.92853	*Lrrc15*
Chemokine (C-C motif) ligand 2	AF065933	14.92853	*Ccl2*
Interferon, alpha-inducible protein	AK019325	14.92853	*G1p2*
Runt-related transcription factor 1	NM_009821	12.12573	*Runx1*
Interferon regulatory factor 7	NM_016850	12.12573	*Irf7*
Collagen triple helix repeat containing 1	AK003674	12.12573	*Cthrc1*
Cytochrome P450, family 7, subfamily b, polypeptide 1	NM_007825	11.31371	*Cyp7b1*
Pleiotrophin	BC002064	11.31371	*Ptn*
Procollagen, type V, alpha 2	AV229424	11.31371	*Col5a2*
Fibronectin 1	BM234360	10.55606	*Fn1*
Chondroitin sulfate proteoglycan 2	NM_019389	10.55606	*Cspg2*
Thrombospondin 1	AI385532	10.55606	*Thbs1*
Membrane-spanning 4-domains, subfamily A, member 4C	NM_022429	10.55606	*Ms4a4c*
Lysyl oxidase	M65143	10.55606	*Lox*
Growth differentiation factor 15	NM_011819	9.849155	*Gdf15*
Dynamin 3, opposite strand	BB542096	9.849155	*Dnm3os*
RNA imprinted and accumulated in nucleus	BB649603	9.849155	*Rian*
WNT1-inducible signaling pathway protein 1	NM_018865	9.849155	*Wisp1*
Secreted frizzled-related sequence protein 1	BI658627	9.849155	*Sfrp1*
Procollagen, type III, alpha 1	AW550625	9.849155	*Col3a1*
Signal transducer and activator of transcription 2	AF088862	9.189587	*Stat2*
2′-5′ Oligoadenylate synthetase-like 2	BQ033138	9.189587	*Oasl2*
Tenascin C	NM_011607	9.189587	*Tnc*
Neural cell adhesion molecule 1	BB698413	8.574188	*Ncam1*
Integrin α5 (fibronectin receptor alpha)	BB493533	8.574188	*Itga5*
Tribbles homolog 3 (*Drosophila*)	BB508622	8.574188	*Trib3*
Gap junction membrane channel protein alpha 1	M63801	8.574188	*Gja1*
Interferon-induced protein with tetratricopeptide repeats 2	NM_008332	8.574188	*Ifit2*
Serine (or cysteine) peptidase inhibitor, clade A, member 3N	NM_009252	8.574188	*Serpina3n*
Lysyl oxidase-like 2	AF117951	8	*Loxl2*
GLI pathogenesis-related 2	BM208214	8	*Glipr2*
2′-5′ Oligoadenylate synthetase-like 1	AB067533	8	*Oasl1*
Tissue inhibitor of metalloproteinase 1	BC008107	8	*Timp1*
Immunoglobulin heavy chain 4 (serum IgG1)	BC008237	0.033493	*Igh4*

cells. Expression of extracellular matrix-related genes, including procollagen type VIII α1, was increased in peritoneal fibrosis model. Inflammatory cytokines including IL-6 were also upregulated. Among these upregulated genes, we focused on secreted proteins. One of them was PTN, which is an 18-kDa secreted protein and has been reported to promote mitogenesis and chemotaxis in cultured cells. Microarray analysis showed that PTN signal in the peritoneal membrane in the CG-injected wild-type mice was upregulated by 11-fold compared with PBS-injected mice (Table 1). Next, we confirmed the increase of PTN mRNA expression in the peritoneum of CG-treated mice by real-time reverse transcriptase-polymerase chain reaction (RT-PCR) analysis (Figure 1b). PTN mRNA in the peritoneum of CG-treated mice was gradually increased and peaked at 3 weeks by 39-fold compared with that in PBS-treated mice at 28 days, and was high until 4 weeks (Figure 1b). Diluted CG, such as 0.03 or 0.01%, induced weaker expression of PTN mRNA than 0.1% CG (Figure 1b). Western blot analysis also showed that PTN protein in the peritoneum of CG-treated mice was gradually upregulated and was highest at 3 weeks by 3.9-fold, as compared with that of PBS-treated mice (Figure 1c). A low concentration of 1:10 diluted CG induced less PTN expression (Figure 1c). Immunohistochemical study showed